Application of Enzymatic Catalysis and Galvanic Processes for Biosensor Development

by

Brian Andrew Zaccheo, B.S.

Dissertation

Presented to the Faculty of the Graduate School of

The University of Texas at Austin

in Partial Fulfillment

of the Requirements

for the Degree of

Doctor of Philosophy

The University of Texas at Austin

August 2011

Acknowledgements

I wish to express my esteem for my research advisor, Dr. Richard M. Crooks, for his mentorship and support over the past four years in his laboratory. When I started my graduate education, the path to take was not immediately apparent, but I feel pride in the innovations and accomplishments that were made possible by his accommodation and counsel.

I would like to thank my committee members, Dr. Karen Browning, Dr. David Hoffman, Dr. Keith Johnston, and Dr. Keith Stevenson for their advice and ideas during my graduate career.

My work here at UT would not have been possible without my fellow group members Dr. Kwok Fan Chow and Dr. Derek Laws. Both entertained my ideas, thoughts, and questions with patience and wisdom, and to them I am grateful.

To my family and friends I extend my deepest thanks. Their conversations, laughter, and support have been invaluable.

Application of Enzymatic Catalysis and Galvanic Processes for Biosensor Development

Brian Andrew Zaccheo, Ph. D.
The University of Texas at Austin, 2011

Supervisor: Richard M. Crooks

Methods for integrating enzyme systems with electrochemical reactions having applications to diagnostic sensing are described. Diagnostic tests that include biological molecules can be classified as biosensors. Existing testing methods often require trained technicians to perform, and laboratory settings with complex infrastructure. The theme of this dissertation is the development of methods that are faster, easier to use, and more applicable for non-laboratory environments. These goals are accomplished in systems using enzymatic catalysis and galvanic processes.

Two biosensors with specific model pathologies have been designed and demonstrated in this study. The first assay senses a DNA fragment representing the Epstein Barr virus and uses enzyme-mediated Ag deposition over a

microfabricated chip. The chip contains a specially designed pair of electrodes in an interdigitated array (IDA). Detection is signaled by a change in the resistance between the two electrodes.

The second biosensor discussed in this study is targeted towards the digestive enzyme trypsin. It is self-powered due to its construction within an open-circuit galvanic cell. In this system, a small volume of blood serum is introduced onto the device over barriers made of protein and Al that block the anode from solution. In the presence of trypsin, the protein gel is rendered more permeable to sodium hydroxide. Adding hydroxide initiates the dissolution of the Al layer, closing the cell circuit and illuminating a light-emitting diode (LED). A relationship was observed between LED illumination time and trypsin concentration.

Biosensors that utilize enzymes to generate or amplify a detectable signal are widely used, and the final project of this study uses a nanoparticle based approach to protect the catalytic activity of alkaline phosphatase (AlkP) from hostile chemicals. By incubating Au colloid with AlkP overnight and adding Ag^{+}, core@shell nanoparticles of $Au@Ag_2O$ can be isolated that show AlkP activity. The resulting enzyme-metal composite material was analytically characterized and demonstrated greater activity in the presence of organic inhibitors relative to either wild type

or Au colloid-associated AlkP without the Ag_2O shell. The stabilization procedure is complete in one day using a one-pot synthesis. This method may provide opportunities to carry out biosensing chemistry in previously incompatible chemical environments.

Table of Contents

List of Tables

List of Figures

List of Schemes

Chapter 1: Introduction

1.1 Application of Enzymes to DNA Biosensing

Detecting biological materials at physiological concentrations is a common and relevant practice in both analytical and biochemical fields. The development of methods, techniques, and devices that accomplish biosensing represents a growing area in the sciences, in both academic and industrial settings. The blood glucose sensor is a good example. In this sensor, glucose is detected electrochemically using the enzyme glucose oxidase to obtain precise measurements almost instantly using minimally invasive methods.[1] Similarly, the home pregnancy test kit is a biosensor that uses enzymes to generate signal for either human chorionic gonadotropin or early pregnancy factor. Both systems detect physiologically relevant biological molecules using enzyme-based detection systems.

Enzymes are catalytically active proteins that accomplish a vast set of reactions. As proteins, enzymes are polymers comprised of multiple amino acid residues. Each amino acid has a side chain group whose structure is unique to the residue. Groups such as imizadole from histidine, hydroxyls from serine and threonine, amines and thiols are available in amino acids to can carry out reactions featuring isomerization, hydrolysis, and electron transfer. Many enzymes have been useful in commercial processes and medicinal applications. For example, amylases break down

starches and create functional materials for biofuels, home cleaning, and industrial applications. With increasing recognition for protein-based catalysis, the scientific literature provides ample evidence of the increased use of enzymes in chemical methods.[2]

Enzymes can function under conditions that vary by source organism.[3] It is common to find multiple versions of the same enzyme in a single organism that catalyze the same type of reaction but under different conditions tailored to individual organs.[4] These different enzymes are collectively called isoforms. A chemical that is a good substrate for one isoform of an enzyme may not work for another from the same organism but could be accepted by an isoform from a different species. While this complicates the incorporation of an enzyme into a sensor, it can be beneficial by selecting an isoform that is compatible with the salts and pH levels appropriate for a specific process.

Biosensors often incorporate enzymes with electrochemical systems. Horseradish peroxidase (HRP) reduces hydrogen peroxide and can oxidize multiple substrates for electrochemical detection.[5] HRP operates via a critical iron-containing protoporphyrin ring that facilitates electron transfer. While HRP generates oxidized species for detection, other enzymes can produce reduced species. Alkaline phosphatase (AlkP) hydrolyzes phosphate groups from substrate molecules to hydroxyl groups.[6] For some substrates, including aminophenol phosphate, ascorbic

acid phosphate, and naphthyl phosphate, the enzymatic products are 1- or 2-electron reducing equivalents.[7] Biometallization is a process in which AlkP-generated reducing equivalents reduce metal ions, typically Ag^{+}, to form a conductive deposit.[8] Detecting Ag metal may be accomplished using several techniques. In large amounts, Ag can mirror a surface for optical detection.[9] Spectroscopic approaches and electrochemical methods like anodic stripping voltammetry (ASV) have also been used to detect Ag.[10] Electrical measurements of resistance can detect Ag when deposited across addressable electrodes or arrays of electrodes.[11]

An interdigitated array (IDA) consists of two interlocking, individually addressable, comb-like electrodes consisting of long parallel strips positioned in close proximity to each other. Optimally the electrodes would be spaced as close together as possible such using nano- or photolithographic manufacturing.[12] IDAs improve the limit of detection in electrochemical sensing through redox cycling. In redox cycling, each electrode is held at potential either oxidizing or reducing to detect the same analyte multiple times.[13] The analyte, being alternatively reduced or oxidized with each collision at either electrode, generates a proportionally larger electrochemical signal for the given amount of analyte than would be possible with direct methods such as chronocoulometry or cyclic voltammetry. Closely-spaced electrodes are useful also as platforms for measuring

the conductivity of deposited materials such as nanowires of silver or polyaniline.[14-17] The key principle for IDAs is to pack many electrodes in close proximity to interact with analytes. IDA platforms are versatile for electrical and electrochemical applications as they offer increased sensitivity by packing a large electrode inside an area having a small footprint.

Biosensors for DNA detection have become increasingly common, with platforms reaching ever lower limits-of-detection. The standard assay for ultrasensitive DNA measurement uses the quantitative, real-time polymerase chain reaction (qPCR) in which a fluorescent dye is incorporated into a reaction mixture with the desired DNA oligonucleotide, appropriate amplification primers, a mixture of free nucleotides, and polymerase enzymes.[18] In PCR, a series of temperature-dependent steps first binds a primer DNA strand onto the analyte strand. Second, the primer is enzymatically elongated with new DNA whose sequence is complementary to the analyte. Finally, the strands are heated to dissociate the copy from the original analyte. This process can be repeated to duplicate the original DNA exponentially. In qPCR, a double-strand specific intercalating dye is present during amplification. By measuring the fluorescence signal during each amplification cycle, it is possible to back-calculate the initial concentration of analyte DNA in the initial sample. As a technique, qPCR is well understood and widely accepted.

However, qPCR is labor and infrastructure-intensive, and thus is not suitable for point-of-care or field-based applications where the availability of specialized equipment and trained technicians is uncertain. Therefore, approaches have been made to develop biosensors for DNA detection that achieve levels close to, or on par with, qPCR that do not use DNA amplification.

There are three main DNA-based DNA detection systems employed in biosensing applications: the sandwich assay, a capture-target assay, or a hairpin assay. These methods are illustrated in Scheme 1.1. The sandwich assay is similar in principle to the enzyme-linked immunosorbent assay (ELISA) where a surface is modified with a "capture" DNA strand via a linker group. The capture DNA has a sequence complementary to the DNA target. After exposure to the target and hybridization, a reporter strand is added. The reporter is complementary to the target and is labeled with another linker group. In the capture-target assay, the capture binds an already-modified target that contains the second linker. This assay is similar to the sandwich but requires fewer steps by foregoing the reporter DNA.

Scheme 1.1

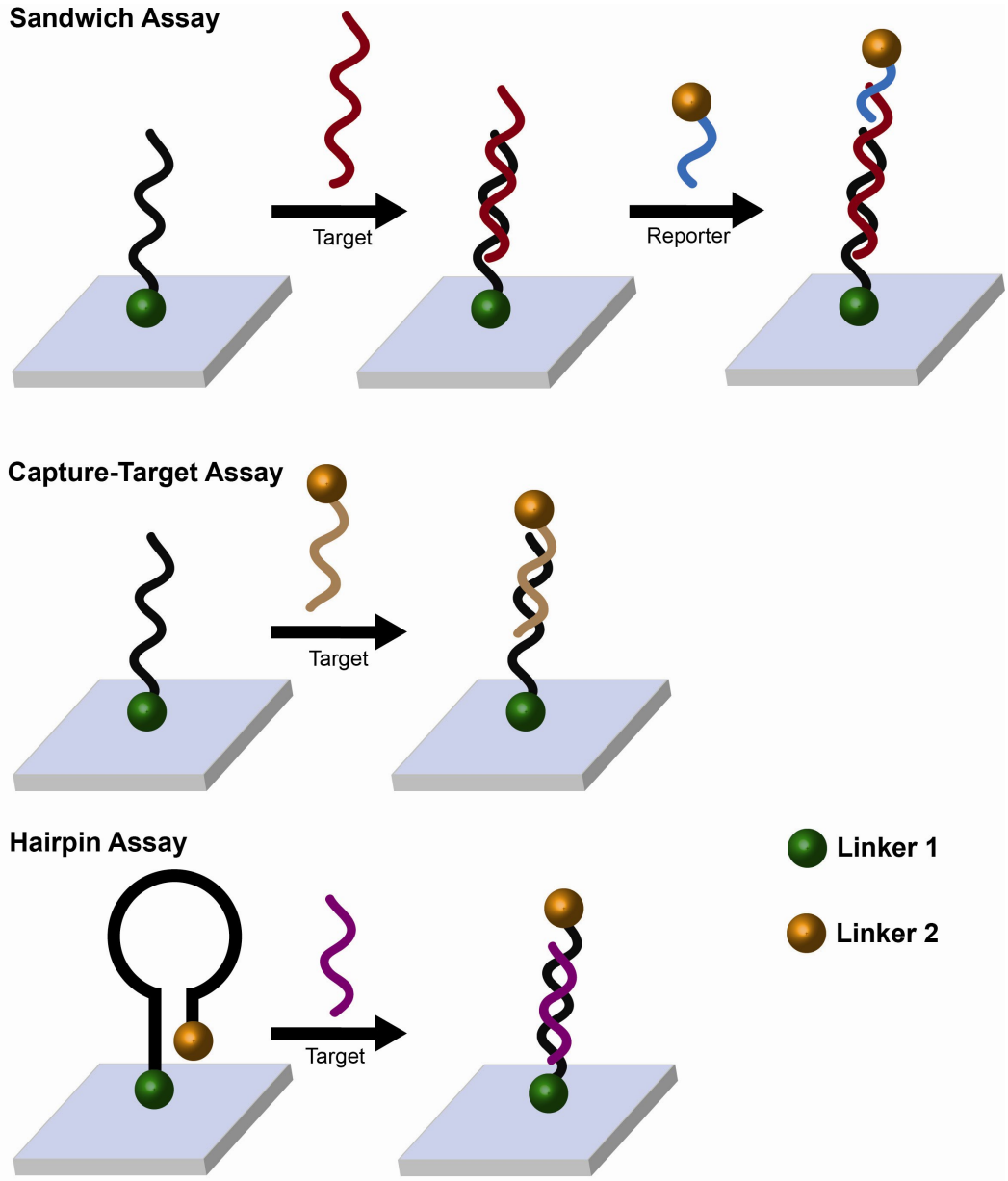
Sandwich Assay
Target
Reporter
Capture-Target Assay
Target
Hairpin Assay
Target
Linker 1
Linker 2

The hairpin assay scheme uses a capture DNA that is self-complementary at both ends. The hairpin is attached to the substrate via one linker group as in the other assays. However, the substrate-bound end sequesters a second linker near the substrate, obscuring it from being recognized in solution. A single-stranded loop whose sequence is complementary to the substrate is positioned between the two linkers. Hybridization with the target DNA opens the hairpin by thermodynamically overwhelming the self-complementary interactions. The end result is the release of the linker group from its bonding near the surface to be solution accessible. The hairpin solution is elegant and uses only 1 modified oligonucleotide to detect an unmodified target. The common element of these hybridization methods is that they employ a second linker group to recruit a detection system.

Reporting and detection systems frequently include the recruitment of nanoparticles, enzymes, antibodies, and catalysts using linking chemistry for colorimetric, immunological, or electrochemical detection. A pioneering work by Mirkin and coworkers used DNA-modified nanoparticles (NPs) in what was termed a “bio barcode” approach to detect DNA at low concentrations without PCR amplification. The analyte DNA was used to recruit a nanoparticle (NP) coated in a secondary DNA sequence – the barcode – that would then be selectively detected via the analyte DNA and bound to a surface. Once bound, barcode DNAs are dissociated from the NP for detection. The liberated barcodes are bound using a

sandwich assay, and labeled with a Au NP. Finally, the Au is enhanced with Ag for visual detection.[19] This approach affords extreme sensitivity, detection on the order of less than dozen molecules, through the use of catalytic Ag reduction and extensive DNA-NP methodology.

Biometallization was first reported using a sandwich assay to recruit AlkP and ultimately deposit Ag onto an electrode for quantification by ASV.[8] A later biometallization work used a sandwich assay for DNA binding and deposited Ag onto capture DNA-modified agarose beads.[20] Beads provide a large surface area and enhance the sensitivity of the device by providing a thermodynamic advantage for detection through a larger amount of capture DNAs on many beads. A disadvantage of using beads is that they are insulating, and so the quantification of Ag required a peroxide treatment to oxidize the zerovalent Ag on the beads into solution for subsequent detection by ASV. Enzymatic biosensors can also take advantage of IDAs to detect the electrochemical response of the substrate in a microchannel. A capture-target assay was used to recruit AlkP onto the walls of a microchannel to generate 4-aminophenol. DNA sensing was quantified by flowing the solution over an IDA and recording the current generated by redox cycling. The observed current varied as a function of the initial target DNA concentration.[21]

To design a sensor that is extremely sensitive for a target DNA, there are several properties to consider. First,

there should be an excess of complementary capture DNA to drive the hybridization and immobilization of the target to the fullest extent possible as per Le Chatlier's principle. Second, the detection scheme should be optimized to take full advantage of sensing events. The biometallization reaction is an excellent reporter to deposit conductive Ag. Pairing biometallization with DNA-modified IDAs provides a large area of capture DNAs in a small space, and by extension localizes Ag deposition to a small area over the tightly-packed IDA. Given the small distances between the electrodes in an IDA, this system can be sensitive by requiring only a small amount of Ag to short the electrode array detected as a change in electrical resistance using a hand-held multimeter.

1.2 Trypsin Detection via a Galvanic Biosensor

Electrolytic techniques, like ASV, use a power supply or a potentiostat to induce reactions in an electrochemical cell. Current passes through the cell by means of charge transfer events between the electrodes and an electroactive species in solution. By contrast to an electrolytic system, a typical galvanic system uses one or more active metals to generate a current by coupling oxidation and reduction reactions in a spontaneous process.[22] The two reactions are often segregated into half-cells. The half cells are connected by a porous salt bridge that supplies ions to maintain charge neutrality during current flow. The

principles of galvanic electrochemistry are essential to the modern world as evidenced by the wide availability of battery-powered devices. A simple galvanic cell is shown in Scheme 1.2 using an Mg anode that oxidizes to Mg^{2+} while Fe^{3+} is reduced to Fe^{2+} at the cathode. The cell potential and current of a galvanic cell may be predetermined by the deliberate selection of anode/cathode materials and the incorporation of resistors, respectively. The flow of current can be indicated several ways. Multimeters can report a value for the cell potential or read the current. Piezoelectric transducers produce sound, and light-emitting diodes (LEDs) emit colored light when current is flowing. LEDs act as electron-to-photon transducers that can operate at moderate currents (>10 mA) and voltages of ~2 V.[23-24]

Scheme 1.2

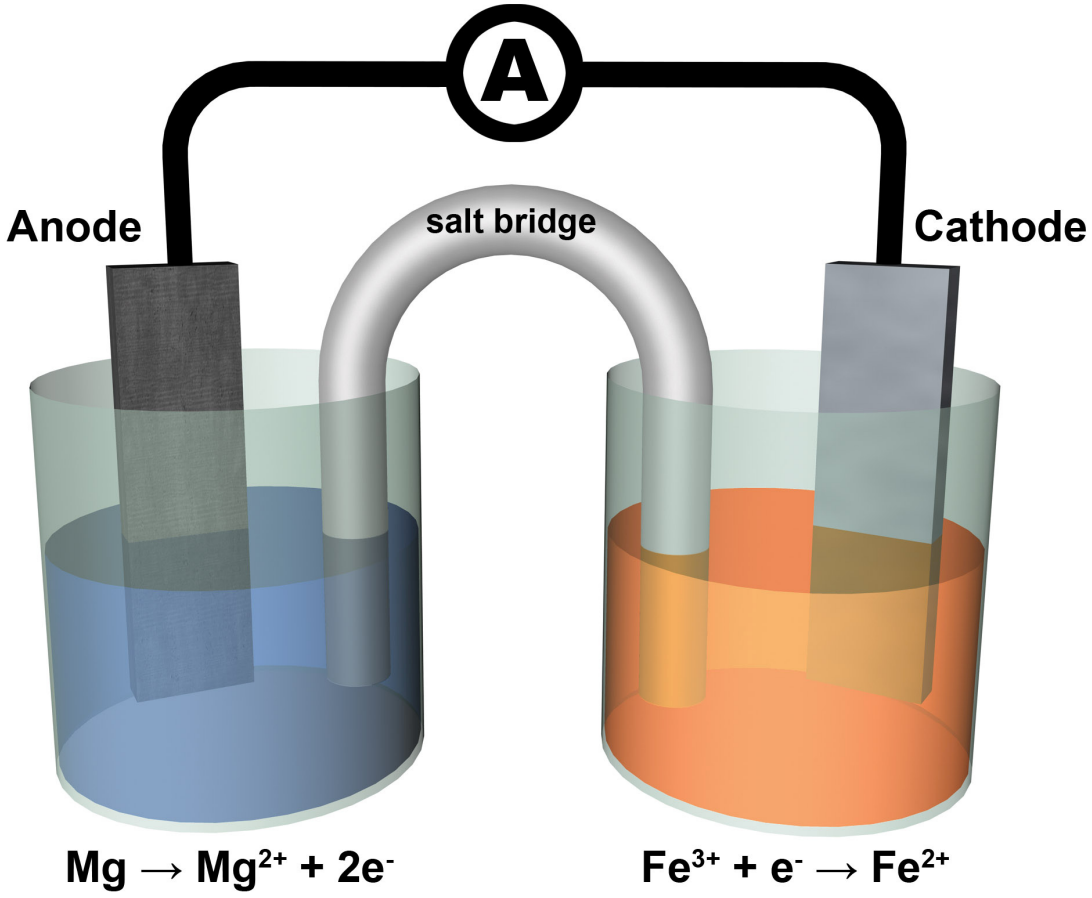

Trypsin is a proteolytic enzyme formed in the pancreas that assists in digestion using a catalytic triad of amino acids to effectively break peptide bonds. It is initially synthesized as the proenzyme trypsinogen, which cleaves into the active protein and an inert segment in a Ca^{2+} dependent process.[25] Under certain conditions, an overabundance of trypsin is produced, damage to the pancreas may occur, and active trypsin leeches out into the blood. The detection of trypsin in human serum has been correlated with the pathology of acute pancreatitis.[26] If not treated and corrected, the condition can be fatal. More specifically, tests showed trypsin levels in pancreatitis patients are elevated 5-fold versus healthy subjects. This difference is small but is important enough to be considered one of several hallmarks for the disease. As a biomarker, trypsin is difficult to detect as it is proteolytic, meaning it can self-cleave or interfere with other proteins that might be involved in detection. Existing immuno- and electrochemical assays use the antigenic and catalytic activities of trypsin, respectively, for indirect detection methods.[27]

Animal proteins are excellent substrates for trypsin, and have useful functional properties including gelation and encapsulation. Gelatin is a trypsin substrate obtained by chemically denaturing connective tissue, bone, or skin into monomers.[28] The monomers reversibly denature when exposed to heat, and upon cooling form extensive hydrogen-bonding

networks that crosslink monomers and trap solvent molecules to form a gel.[29]

In commercial and industrial applications, sodium hydroxide has long been used as a cleanser to break down clogs in pipes and drains. Milk proteins are known foulants to metal surfaces, as proteins can adsorb to surfaces. The dairy industry has reported that caustic cleansers, such as sodium hydroxide, compound the problem by forming rigid, proteinaceous solids.[30] To assist the dairy industry, Mercadé-Prieto and others have performed rigorous analyses of the dynamics of caustic-induced gelation of dairy proteins in whey.[30-33] Whey has two main proteins: a-lactalbumen and b-lactoglobulin. Both undergo denaturation when exposed to temperatures in excess of 60 °C and alkalinity above pH 10. The second protein, b-lactoglobulin, has been studied independently for its gelling ability and susceptibility to trypsin degradation. Together, gelatin and b-lactoglobulin represent typical proteins that are substrates for trypsin. An important difference between the two proteins is that gelatin is degraded by hydroxide through alkaline hydrolysis, b-lactoglobulin forms a tough gel in the presence of hydroxide that resist degredation.[34]

Trypsin activity is quantified in Units by following the cleavage of chromogenic precursors in time-resolved colorimetric assays.[35] Colorimetric assays are well characterized, but generally limited to large amounts of trypsin. Sensitive assays using ELISA or electrochemical

methods are effective but intricate. A previously published detection scheme uses trypsin to de-encapsulate a second enzyme, glucose oxidase (GOx) so that solution glucose can be reacted to produce peroxide for detection with a Pt electrode.[27] Similarly, trypsin was reported to be detecting using a gelatin-passivated IDA; trypsin digests the protein layer, making the electrode accessible to electrolyte for solution-phase conductivity measurements.[36] These methods are quantitative but require sophisticated infrastructure. Using a rapid-onset pathology like pancreatitis, it is desirable to design a diagnostic sensor that works quickly and simply. Molecular recognition systems, like ELISA assays, that detect trypsin are also vulnerable to digestion by trypsin. Trypsin-mediated cleavage generates a colorimetric or fluorescent signal as shown by Lefkowitz et al, in which a fluorphore-tagged polypeptide that has a overall negative charge is cleaved by trypsin in buffer to yield a fluorescent tagged peptide fragment with a net positive charge.[37] Resolving the fragment on a system of three polyacrylamide gels detects the fluorescent fragments produced by trypsin at 0.2 ng/mL. This method was also shown to detect trypsin if whole blood or blood plasma was added after the cleavage reaction was complete.

Designing an assay that is not impeded by proteolytic digestion requires a different approach where proteolysis induces an obvious signal. The sensor should respond to small amounts of trypsin, and the signal should be obvious

for applications outside large clinical settings. The gating of a galvanic cell to trypsin-mediated proteolysis would provide an obvious signal by sudden closure of a circuit. Circuit closure can be indicated by the emission of light, sound, or the actuation of a motor. Additionally, building a sensor whose platform is a galvanic cell precludes the need for external power for applications and settings in which the laboratory infrastructure is modest.

1.3 Enzyme Stabilization with Nanoparticles

Enzymes have been isolated that catalyze many useful reactions. The possibilities for enzyme implementation in consumer and industrial applications are numerous, but they are counterbalanced by both the difficulty in obtaining sufficient quantities of enzyme and keeping the enzyme active to accumulate a meaningful amount of product. The latter concern will be addressed herein and has been explored previously in the biochemical and analytical literature.[38-39] Protective approaches have been identified that claim to extend the catalytic lifespan of an enzyme, to protect against changes in pH, and to preserve protein structure during drying and rehydration. Of these methods, the most widely discussed is the sol-gel enzyme encapsulation technique.[40] Sol-gel encapsulation of proteins and enzymes occurs in two steps. First, an alkyl-silane precursor, often tetraethyl orthosilicate, is combined with crosslinkers in solution. Second, the sol is combined with

the protein solution, and the resulting mixture begins to rigidify in a process that can take, depending on the conditions used, up to a month to form a set gel. After solidifying, the gel is washed extensively to remove unbound enzyme. Finally, the gel is ready for use as a slab or treated to yield packing beads, pulverized powder, or other preparations to deliver silicate-entrapped enzyme. An advantage of the sol-gel entrapment approach is that the jelling can be used to make conformal layers that adhere to substrates to essentially give a porous film of entrapped enzyme.[41] The pore size is controllable in part through the deliberate selection of the silane precursor and the crosslinking conditions. The ideal sol-gel is porous enough to allow mass transport of substrate and product, but not so porous to allow a large efflux of the enzyme.[42] In the case of the electron-carrying, heme-containing protein cytochrome c (cyt c), it was observed that direct encapsulation was destructive to the protein as determined by the loss of the Soret band in UV-vis (a sharp absorbance at ~440 nm) as characteristic for ordered Fe-ligand interactions found in the protoporphyrin ring.[43] The denaturation of cyt c was resolved by adding Au colloid as a stabilizing agent. As a demonstration of the high porosity of the gel, the Soret band could be selective decreased and restored by the passage of NO or Ar gas over the sol-gel. The loss of the Soret band indicates the binding of NO to the Fe center in the heme, disrupting the Fe/ligand interaction. The

restoration of the Soret band with flowing Ar demonstrates the porosity of the sol-gel and the preservation of cyt c structure.

Other nanoparticle-inclusive approaches towards the protection and stabilization of enzymes have been reported. An adaptation of the sol-gel approach modifies surface-exposed primary amines on a protein with alkyl silanol groups to gradually coat individual proteins with a sol-gel layer to produce single-enzyme nanoparticles.[44] An approach was published in which enzymes and proteins are entrapped within or onto metal nanoparticles by reducing metal salts with reducing agents or electroactive amino acids to form metal-encapsulated proteins.[45]

Acid phosphatase was encapsulated by directly reducing Au^{3+} or Ag^{+} in solution with the enzyme using Zn^{0}.[46] In their work, the reduction yields a powder that is reported to be enzymatically active. This advantage of this method is that direct reduction with Zn^{0} powder is nearly instantaneous. This is in contrast to the weeks-to-months timeline required for some sol-gel preparations.[40-41]

The synthesis of a noble-metal nanoparticle that entraps an enzyme via adsorption or surface interactions requires careful consideration. For example, metal salts often have an inhibitory effect on the enzyme, or the protein may require a pH at which the metal is not stable.[6] A balance is required between conditions that support the

catalytic and structural integrity of the enzyme alongside salts and reducing agents that do not inhibit the enzyme.

Enzyme entrapment and encapsulation into solids, gels, or hybrid materials has the promise of protecting the enzyme from denaturation. Ideally the enzyme will be confined inside a relatively small cavity. Confinement would prevent the protein secondary structure from being heavily altered by chemicals. By analogy to this method, consider the packing of sensitive electronic components or technical instruments into molded-foam padding. With packing, there is physical resemblance between the shape of the component being protected and the enclosure itself. Applying this model to enzymes, the likelihood of enzyme damage is decreased by limiting the area for which the protein can shift. Surrounding an active wild type (WT) enzyme inside a material, for example a sol-gel, should prevent denaturation. The implied benefit of this approach is to extend the range of environments in which an enzyme remains catalytically active. Chemical denaturants like urea and sodium dodecyl sulfate (SDS) are employed in protein characterization methods to eliminate the interactions inside and between proteins (including alpha helices and beta pleated sheets) to enhance separation methods like gel electrophoresis.[47]

Enzyme entrapment can be protective against inhibitory chemicals. One difficulty with inhibitors is that, like reaction conditions, the efficacy of inhibition will vary

heavily from one organism and source cell line to the other.[48] One isoform may be strongly inhibited by a given chemical, but another isoform may be activated and behave better in its presence. Using alkaline phosphatase (AlkP) as a subject for inhibition provides several options for potential inhibitors. The literature has shown that denaturants like urea and SDS can be effective, as well as more targeted chemicals like levamisole, L-phenylalanine, and homoarginine.[49-52]

1.4 Research Summary and Accomplishments

My dissertation focuses on the development of techniques and methods towards diagnostic biosensors that feature enzyme mediated catalysis and galvanic processes. Two different biosensors are described herein: DNA detection using a capture-target assay, and a protein sensor for the digestive enzyme trypsin that is self-powered. A third project stabilizes AlkP with core@shell Au@Ag_2O nanoparticles with potential applications for biosensing. A central theme of all three projects is that each system is designed to complement previous methodology by being equally if not more effective while providing a marked improvement in terms of being faster to perform, requiring less laboratory infrastructure, or applicable in a previously undemonstrated way.

Chapter 3 describes a DNA sensor for an analogue of the single-stranded DNA genome of Epstein-Barr virus. This

sensor uses enzymatic catalysis to biometallize an IDA and for ultrasensitive DNA detection. The target DNA was detected a concentration of 1 aM, approximately 24 molecules of target, to give PCR-like sensitivity in an assay that is performed using a modified IDA on a disposable chip, a handheld multimeter, and minimal laboratory infrastructure. The sensitivity is attributed to optimization of biometallization by performing the reaction over an IDA, separating the enzymatic generation of reducing equivalents from Ag deposition, and the use of Tollen's reagent (silver diammine) as the Ag^{+} source. Tollen's is well suited for Ag deposition on glass substrates such as the interstitial area between the IDA.

Chapter 4 describes the development and design of a biosensor for the digestive enzyme trypsin based on the enzymatic degradation of a protein gel and Al foil gate in an open circuit galvanic cell. The action of trypsin on the protein layer renders the gel more permeable than the native gel, and when subsequently exposed to hydroxide (an etchant for Al), the trypsin-exposed gels allow hydroxide to dissolve the Al faster than non-exposed gels. When the Al barrier is compromised by hydroxide, the circuit for the galvanic platform is closed, the cell discharges, and an integrated LED illuminates. To demonstrate the efficacy of this sensor for the model pathology of acute pancreatitis, a detection method was demonstrated using trypsin in equine serum. A relationship between the illumination time of the

LED and the concentration of trypsin in the analyte was observed. This gives the system a quantitative ability.

Chapter 5 describes the stabilization of alkaline phosphatase (AlkP) with Au@Ag_2O colloids. The enzyme-nanoparticle conjugates were analytically characterized. Transmission electron microscopy (TEM) and energy dispersive spectroscopy (EDS) report morphological properties of the conjugates. UV-vis and x-ray photoelectron spectroscopies (XPS) detail optical and chemical properties. The activity of the enzyme was monitored with a quantitative activity assay tracking the hydrolysis of *p*-nitrophenol phosphate to the strongly colored *p*-nitrophenol. Activity measurements were taken under several conditions. AlkP was exposed to citrate-capped Au colloid in buffer and found to associate strongly to the particles. Subsequent addition of an Ag^+ solution results in the formation of a Ag_2O shell over agglomerated Au colloids. The assembly of these enzyme-metal conjugates, referred to as AlkP-Au@Ag_2O, occurs more rapidly than sol-gel based entrapment.[40-41] Additionally, it was possible to quantify the extent of active enzyme association within the metal agglomerates. AlkP-Au@Ag_2O tolerates inhibitory organic molecules better than wild type or surface-adsorbed AlkP. Protection from inhibition is attributed to the Ag_2O shell. Potential applications include biosensing and molecular biology methods.

Chapter 2: Experimental

2.1 Chemicals

Chemicals used and described in this work are detailed in their individual chapters.

2.2 Techniques

2.2.1 Photolithography and chemical etching

Fabrication of the IDA electrodes used in this work employed photolithography and wet chemical etching of commercially-supplied Au-coated glass sides having a 10 nm Cr adhesion layer. To produce the desired pattern of two interlocking electrodes, leads, and contact pads, the slides were processed in multiple steps as illustrated in Scheme 2.1, in which layer thicknesses are not to scale. First, the slides were prepared for patterned by extensive cleaning with piranha solvent (made at a ratio of 7:3 conc. H_2SO_4 and 30% H_2O_2) followed by transportation into a low-UV clean room. Next, as shown in part ii, a layer of positive photoresist was applied via spincoating. This material contains a photo-sensitive polymer that is applied as a film to a specific thickness and baked into place until dry.

Scheme 2.1

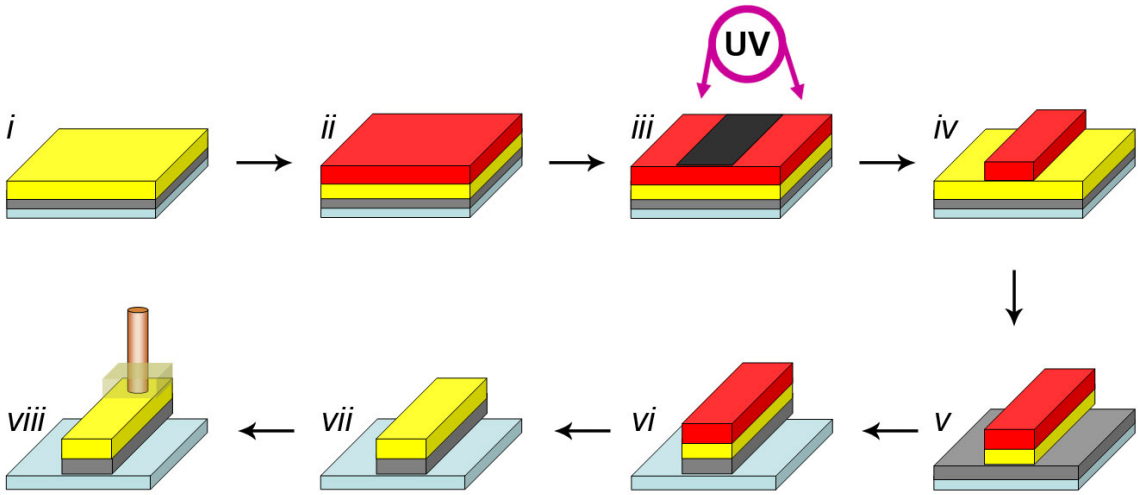

Once set, a photomask bearing an opaque design corresponding to the desired electrode pattern is physically contacted to the set photoresist and UV radiation is applied through the mask as shown in part iii. Following irradiation, the UV-destabilized photoresist is removed with a proprietary developer solution, as seen in part iv, to yield a Au surface passivated with photoresist in the shape of the photomask pattern. Chemical etching of the Au and Cr is accomplished with solution-phase etchants as shown in parts v and vi to expose the underlying dielectric around the electrode. Wet chemical etching uses solvents with reactive species that either dissolve or undergo galvanic exchange with the material to be etched. This exposes the underlying substrate on areas not covered by a blocking agent such as photoresist.[53] Photoresist is removed from the device, typically with acetone or piranha as seen in part vii. Finally, contact wires are affixed using Ag adhesive, shown in part viii, to yield an addressable, patterned electrode. Preparation of electrodes by this method allows for the fabrication of a multitude of patterns and sizes that can be optimized for the selected application. Additionally, the use of Au as the electrode material allows for facile surface modification via self-assembled monolayer (SAM) methods that feature thiol groups.

2.2.2 Materials Characterization with Energy Dispersive Spectroscopy and X-ray Photoelectron Spectroscopy

Morphological and compositional examination of metal films and particles less than 1 μm can be obtained from electron microscopy. Field-emission scanning electron microscopy (SEM) uses electrons to irradiate the surface of a sample. Surface atoms exposed to the incident electrons eject secondary, inner-shell electrons that are collected by a detector to provide a spatially-resolved image. Features larger than 50 nm may be visualized by SEM. The image provides information about the morphology of the substrate being irradiated. A valuable side-effect of this process is the generation of characteristic X-rays. X-rays are emitted when outer shell electrons fill the vacancies in the inner shell.[54] The energy of the X-ray is dependent upon the atomic number and the type of transition. Characteristic X-rays were reported by Moseley in 1913[55] and subsequent work has fully identified the expected X-ray energies correlated to the element and shell transitions that cause emission. Energy dispersive spectroscopy (EDS) is the technique in which elemental analysis of a sample is collected using the X-ray emission upon electron beam irradiation. EDS detectors can collect information about the entire energy spectrum simultaneously to give elemental composition in either qualitative relative frequencies or with additional interpretation for quantitative abundance in atomic percentage. Rastering the incident electron beam over a

surface and measuring the X-ray emissions from each point creates a spatially-resolved element map. Element maps can use false color to represent different elements to present compositional images of metal films, patterned electrodes, surface features, and even nanoparticles.

Similar to EDS is a complementary technique involving the irradiation of a sample by a beam of X-ray photoelectrons called X-ray photoelectron spectroscopy (XPS). In XPS, a monochromated, high-energy incident X-ray source irradiates the sample to result in the ejection of electrons from surface atoms via the photoelectric effect.[54] By analogy to EDS, the result of the X-ray colliding with a surface atom is the ejection of several electrons across multiple electron shells.[56] By selecting X-ray energies appropriate for a desired element and measuring the energies of ejected electrons, a complex spectrum of photoelectron lines at different and unique binding energies is revealed. The signal that is detected reports the intensity of electrons at specific binding energies unique to each element. Binding energies vary by element, oxidation state, and even the local environment of ligands surrounding the atom.[57] In this manner, XPS delivers more chemical information than EDS. It is worth noting though that the sampling depth of XPS is generally limited to ~10 nm of the sample, as opposed to ~50 nm with EDS. High-resolution XPS spectra for individual elements present one or two peaks when looking at the regions corresponding to the most

intense electron ejections. XPS signals for Au are obtained at binding energies corresponding to the 4s through 5p atomic orbitals, though the highest signal is obtained for 4f.[58] Two peaks are observed in the energy region for Au 4f that are labeled as $4f_{7/2}$ and $4f_{5/2}$. The 7/2 and 5/2 are the j values[57] seen in the 4f orbital and effect the signal such that the binding energy of Au $4f_{7/2}$ is 3.67 eV less than $4f_{5/2}$.[58-59] Information about elemental binding energies and their shifts is available through reference books and a database administered by the National Institute for Standards and Technology (NIST).

EDS and XPS may be considered complementary techniques in that they both provide elemental analysis data following sample irradiation and the analysis of emitted radiation. EDS uses an incident electron beam to eject electrons, and then analyzes the x-rays emitted when those electron vacancies are filled. By contrast, XPS uses an x-ray photoelectron source to eject electrons and analyzes the ejected electrons for analysis. Whereas EDS is used to discern only what elements are present, XPS reports the elements that are present and, for some elements, information on their chemical environment. Both techniques require samples to be to be examined under vacuum (ultra-high vacuum for XPS) and work best for conductive materials. EDS and XPS provide valuable information for materials characterization and analysis.

Chapter 3: Detection of an Epstein-Barr Genome Analog at Physiological Concentrations via the Biometallization of Interdigitated Array Electrodes

3.1 Synopsis

This chapter describes a simple DNA sensor having a detection limit of about 24 oligonucleotides and that operates without the need for PCR amplification. The sensor platform is based on an interdigitated array (IDA) of electrodes. The electrodes are modified with DNA capture probes, which are complementary to an analog for the Epstein-Barr genome, and then exposed to an alkaline phosphatase-labeled target. The enzyme catalyzes the formation of L-ascorbic acid, which reduces Ag^+ in solution to yield conductive Ag filaments that span the gap between the electrodes of the IDA. Resistance measurements, made with an inexpensive, hand-held multimeter, signal the presence of the target. The sensor response is insensitive to the presence of a large excess of non-complementary DNA sequences.

3.2 Introduction

In this chapter we report a method for directly detecting modified, single-stranded DNA targets at concentrations normally requiring amplification by polymerase chain reaction (PCR). The time required for detection is on the order of 24 h and the laboratory

infrastructure required is minimal. The operation of the sensor is illustrated in Scheme 3.1. First, a DNA probe is immobilized onto the electrodes of an interdigitated array (IDA). Second, the sensor is exposed to the biotin-labeled, complementary target. Third, the hybridized target is labeled with streptavidin-conjugated alkaline phosphatase (AlkP). Fourth, a solution of L-ascorbic acid 2-phosphate (AsAP) is added, which is converted to L-ascorbic acid (AsA) by the enzyme. Fifth, an electrochemical reaction begins when Tollen's reagent is introduced, resulting in silver deposits that connect the electrodes of the IDA. Finally, the presence or absence of the DNA target is determined via a simple resistance measurement. Using this approach, we have been able to detect concentrations of target as low as 1 aM in the presence of a large excess of potentially interfering, non-complementary DNA.

Scheme 3.1

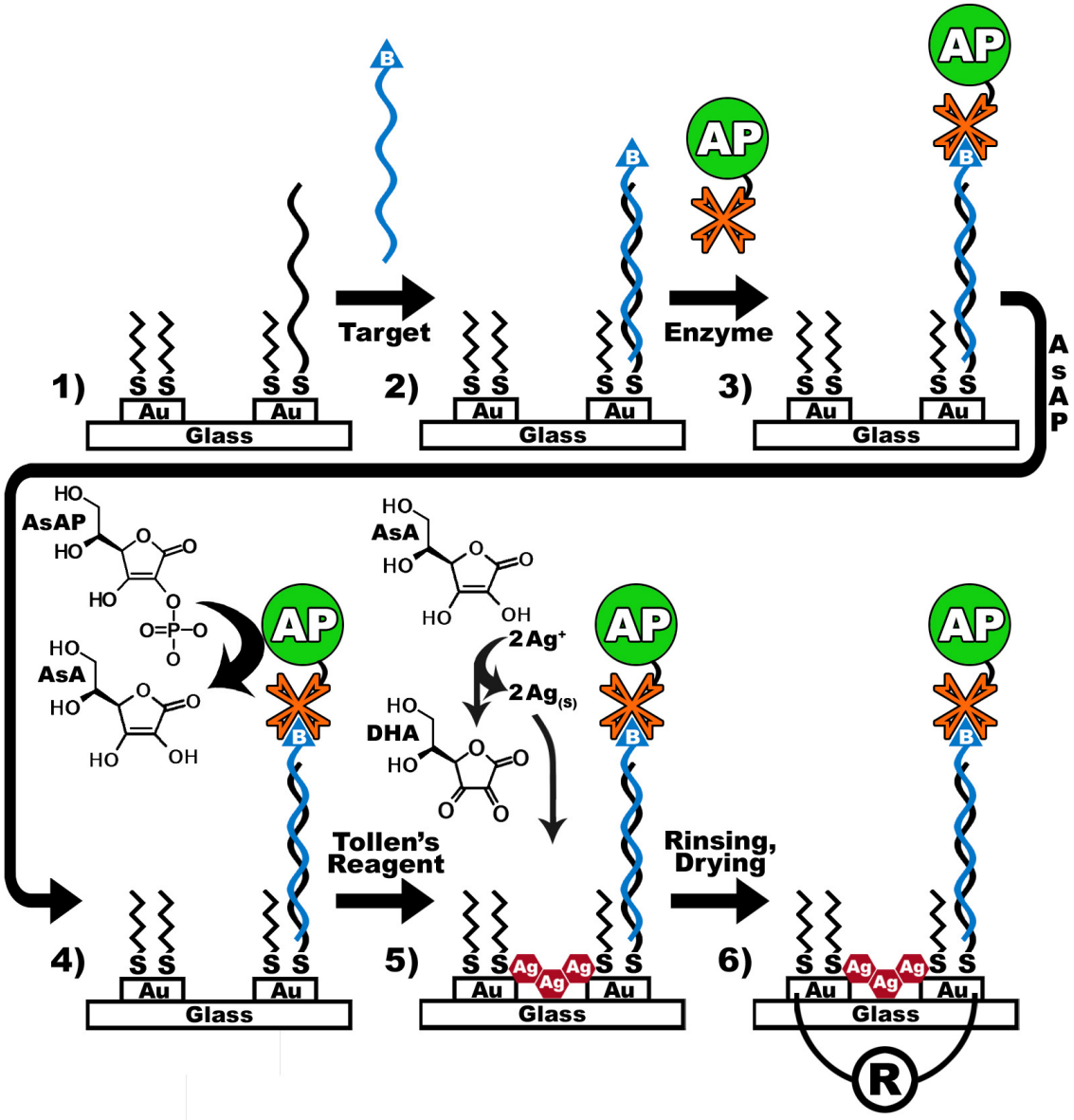
1)
2)
3)
4)
5)
6)
Target
Enzyme
ASAP
Tollen's Reagent
Rinsing, Drying
AP
B
Au
Glass
S S
AsAP
AsA
DHA
HO
OH
O=P–O
2Ag+
2Ag(s)
Ag
R

Sensors related to the one discussed here have been described previously. For example, DNA sensors have been developed in which the binding of target oligomers lead to biometallization. This process is initiated by an enzyme that generates reducing equivalents, which in turn convert metal ions in solution to an insoluble, conductive metal (usually Ag).[60] The deposit may then be detected and quantified by stripping voltammetry.[60-63] Fritzsche and coworkers carried out biometallization between two parallel electrodes to evaluate percolation thresholds of Ag nanoparticles using atomic force microscopy (AFM).[64] Immunoassays using biometallization have also been reported using antibody-conjugated enzymes and stripping voltammetry.[61,63] In contrast to these previous studies, biometallization here is detected by measuring the resistance between parallel electrodes rather than by stripping voltammetry.

Silver deposition has also been used by Fritzsche and Mirkin to amplify the presence of target DNA labeled with Au nanoparticles that catalyze Ag electroless deposition.[9,11,14,65-66] This approach can be designed so that the deposited Ag spans an insulating gap between one or more closely spaced electrodes, thereby reducing the resistance between them.[67] This is the general approach we have adapted to the device reported here.

Enzymes are sometimes used in biosensors to chemically amplify their output signal and hence lower the limit of

detection.[68] In such schemes, the enzyme is used as a label that generates many detectable products tracing back to a single target. Enzymes used for this purpose are robust and have high turnover rates. One such enzyme is alkaline phosphatase (AlkP). Substrates for AlkP include 1-naphthol phosphate[69] and *p*-aminophenol phosphate (pAPP).[21] Both substrates hydrolyze rapidly in the presence of AP to yield electroactive species, but the former has poor solubility in water and the latter slowly hydrolyzes even in the absence of the enzyme.[21] Alternatively, L-ascorbic acid 2-phosphate (AsAP) is also catalytically hydrolyzed by AlkP to L-ascorbic acid (AsA), but it is significantly more stable in water than pAPP.[70-71] Accordingly, we have chosen to use AsAP in the present study.

Circulating nucleic acids (CNAs) are extracellular lengths of DNA or RNA found in human blood plasma and serum. They are thought to originate from abnormal apoptotic processes, necrosis, and various pathologies.[72] Healthy individuals have average serum CNA concentrations of ~36 ng/mL, but this value depends on a variety of both endogenous and exogenous conditions.[73-74] In some cases, the Epstein-Barr virus (EBV) can manifest nasopharyngeal carcinomas.[75] These carcinomas actively produce and leach copies of the viral genome into the blood at concentrations greater than 5.9 copies per microliter, approximately 10 aM, as determined by quantitative real-time PCR.[76] Using the established pathology of EBV, it is possible that carcinoma

cases may be suitable as a focus for biosensor development given the relatively small signal and high CNA background. Accordingly, we have chosen a target symbolic of EBV.

In this chapter we present a chip-based sensor designed to directly detect single-stranded DNA. This system has a detection limit of 1 aM that circumvents PCR amplification by coupling an IDA electrode design[77] with biometallization. Detection was possible for the target at concentrations lower than those reported from EBV carcinomas, even in the presence of non-complementary DNA at concentrations corresponding to the endogenous CNA levels of healthy individuals. Following biometallization in the presence of target, the resistance of the IDA was typically lower than 5 k . In contrast, negative control experiments using a non-complementary capture probe resulted in resistance exceeding 40 M . Thus, the detection signal, resistance, is at least four orders-of-magnitude lower in the presence of the target. Importantly, the only equipment required to distinguish the presence (1 aM) and absence of target is a hand-held multimeter.

3.3 Experimental Section

Chemicals. Photoresist (AZP4620) and developer (AZ421K) were purchased from May's Chemical (Chicago, IL.) A photoresist adhesion promoter (SurPass 3000) was purchased from DisChem, Inc. (Ridgway, PA). Gold-coated glass microscope slides having a Cr adhesion layer were purchased

from EMF Corporation (Ithaca, NY). Conductive glue (Silver Adhesive 503) was purchased from Electron Microscopy Sciences (Hatfield, PA). 1-Hexane thiol (97%) was obtained from Alfa Aesar (Ward Hill, MA). Silver nitrate (99.85%) and bovine serum albumin (BSA) were purchased from Arcos Organics (Morris Plains, NJ). L-Ascorbic acid 2-phosphate hydrate sesquimagnesium salt (AsAP), ammonium cerium nitrate, streptavidin-conjugated alkaline phosphatase, salmon testicular DNA, and PerfectHyb Plus hybridization buffer (henceforth referred to as hybridization buffer) were purchased from Sigma. Tris(2-carboxyethyl)phosphine hydrochloride (TCEP), was obtained from Thermo Fisher Scientific. Aqueous solutions were prepared using 18 M -cm water from a Millipore Milli-Q system (Billerica, MA). All chemicals were used as received.

DNA oligomers were custom synthesized by Integrated DNA Technologies (Coralville, IA). The capture DNA probe contained a 5'-thiol modification, a six-carbon spacer, a triethylene glycol spacer, and a twenty-nucleotide sequence: CAAGACAGCACTACATCCCA-3'. The target nucleotide contained a 5' biotin modification, a 5-thymidine spacer, and the twenty nucleotide sequence: TGGGATGTAGTGCTGTCTTG-3', which corresponds to bases 72027-72047 of wild type EBV (GenBank Accession No. AJ507799).[75] Rinsing buffer was used to clean the devices and consisted of 5 mM TRIS base and 5 mM Na_2SO_4 adjusted to pH 7.4 with H_2SO_4. A non-complementary, negative control oligomer contained a 5'-thiol modification, a six-

carbon spacer, and the nucleotide sequence: GCGCGAACCGTATA-3'. Similarly, a positive control oligomer contained a 5'-thiol modification, a six-carbon spacer, a triethylene glycol spacer, the twenty-nucleotide sequence: CAAGACAGCACTACATCCCA, and a 3' biotin.

Characterization. Electron micrographs were obtained using a LEO 1530 scanning electron microscope (SEM) with a GEMINI field-emission column (Carl Zeiss). Energy dispersive spectroscopy (EDS) data and maps were compiled using EDS2008 software from IXRF Systems (Houston, TX). Electrical measurements were made using a Fluke 79 Series II digital multimeter. Plasma treatment was performed in a PDC-32-G plasma cleaner (Harrick Plasma).

IDA fabrication. Electrodes were fabricated photolithographically by patterning photoresist onto Cr-primed, Au-coated glass and then chemically etching those areas not protected by the photoresist. Slides were first cleaned by immersion in fresh piranha solution (3:1 mixture of conc H_2SO_4 to 30% H_2O_2) for 10 min, and then rinsed several times with de-ionized water. All photolithography was performed in a low-UV light clean room. Substrates were rinsed with water, and mounted on a spin coater. Adhesion promoter was applied using a syringe at a rate of 1 mL/s for 30 s onto slides spinning at 500 rpm. Following 30 s of rinsing with water, the slides were spun dry at 2000 rpm for 1 min. Sufficient photoresist to cover the surface was applied manually to the substrate. Photoresist was spread at

2000 rpm for 1 min, followed by a 2 min bake on a 90 °C hotplate and then a second bake on a 110 °C hotplate for 3 min. At this point, the substrates were mounted in a mask aligner for hard-contact UV irradiation for 7 s. The photomask pattern consisted of 100, 2 mm-long interdigitated electrodes having 10 µm (nominal) lines and spaces leading to 1.5 mm by 2 mm contact pads. After irradiation, the exposed photoresist was stripped by immersion in developer with gentle agitation for 45 s. The developed substrates were rinsed with water and dried with compressed air. Slides were prepared for chemical etching by 30 s of plasma treatment followed by 5 min on a 110 °C hotplate to remove solvent. Unwanted Au was removed from each slide by immersion in an aqueous solution containing 8% (w/v) KI and 2% (w/v) I_2. Slides were then rinsed and immersed in a Cr etchant containing 9% $(NH_4)_2Ce(NO_3)_6$(w/v) in 6% $HClO_4$ (v/v).[53] Photoresist was removed by sequentially washing with acetone, absolute ethanol, water, and finally piranha. Copper lead wires were affixed to the device contact pads using Ag adhesive and secured with an insulating epoxy as shown in Scheme 3.2.

Scheme 3.2

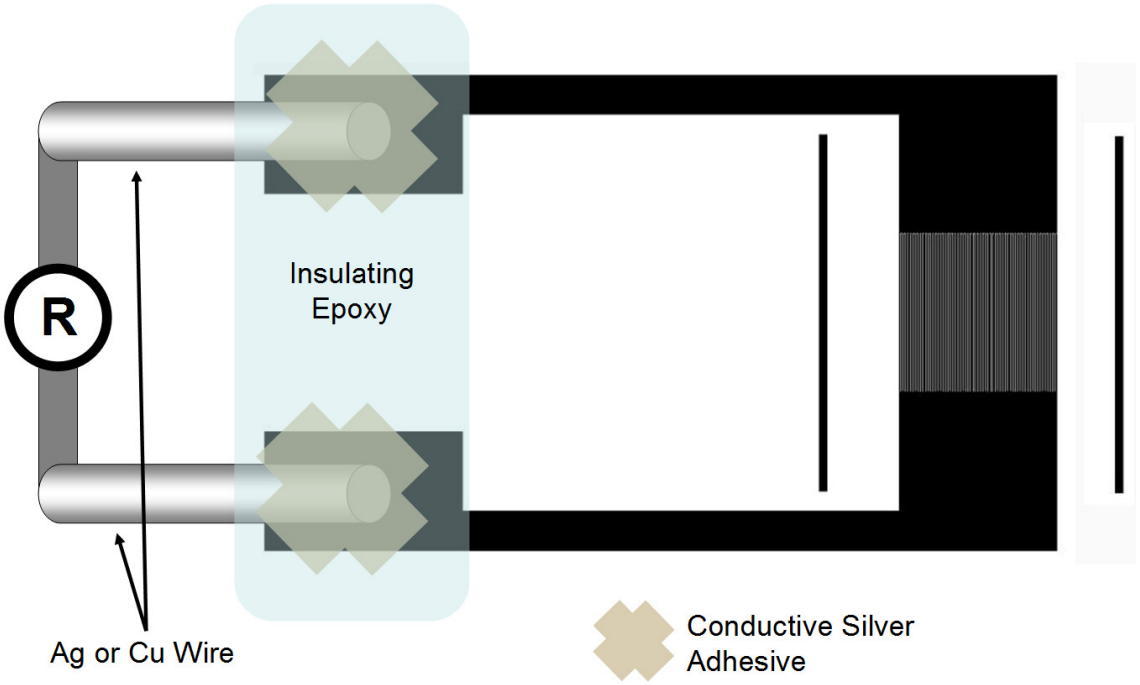
R
Insulating
Epoxy
Ag or Cu Wire
Conductive Silver
Adhesive

Short circuits were removed by applying 40 V ac for 1 min. Finished devices were tested by measuring the resistance between electrodes, and those having resistances > 40 M were retained for experiments. IDAs were stored under vacuum in a desiccator until needed.

Electrode modification. The surfaces of IDAs were modified with capture DNA and then backfilled with an alkylthiol using the following procedure. First, the device was cleaned in a plasma cleaner for 30 s, and then 40 µL of 1 µM capture DNA in 1 M HEPES buffer with 5 mM TCEP at pH 7.0 was applied to the IDA. Next, the device was incubated for 1 h at 23 ± 3 °C inside a closed Petri dish. The IDA was then gently washed with 10 mL of rinsing buffer and then dried under a gentle stream of N_2. A 40 µL drop of 1 mM 1-hexane thiol was then applied to the IDA and incubated for 1 h. Finally, the device was washed with rinsing buffer, dried under N_2, and then used immediately.

Biometallization. As illustrated in Scheme 3.1, the preparation and use of an IDA for target DNA detection occurs in multiple phases. Unless otherwise noted, all processing steps were carried out at 23 ± 3 °C. The modified IDA was exposed to 40 µL of biotinylated target at concentrations of 1 fM, 100 aM, 10 aM, or 1 aM, and incubated for 2 h in a humidity chamber. Target DNA was prepared for use by serial dilution into either neat hybridization buffer or hybridization buffer containing 36.3 ng/mL salmon testicular DNA. After hybridization, the device

was washed with 10 mL of rinsing buffer and dried with gently flowing N_2. Next, the electrode was covered with 40 µL of 0.1 mg/mL streptavidin-conjugated AlkP in 50 mM TRIS base, 0.5 M Na_2SO_4, 1 mM $MgSO_4$, 0.1% (v/v) Tween-20, and 1 mg/mL BSA at pH 7.4. After 15 min the electrodes were rinsed and dried. The IDA was spotted with 10 µL of 10 mM AsAP in 50 mM TRIS base, 1 mM $MgSO_4$ (pH 8.0), and returned to the humidity chamber for 1 h. Ten minutes prior to removing the device, Tollen's reagent was prepared and used without dilution.[78] Briefly, NH_4OH was added to 10% (w/v) $AgNO_3$ until the solution changed from colorless to brown. Then, an additional small volume was added dropwise until the solution was colorless again. Finally, the solution was back-titrated with additional 10% $AgNO_3$ until a slight brown suspension was formed. When the AsAP incubation was complete, the electrode was placed on a 40 °C hotplate for 5 min. A 10 µL drop of Tollen's reagent was placed on the IDA, and the device was returned to the humidity chamber for an additional for 2 h. The device was rinsed with water, cleaned with gently flowing N_2, and dried overnight in air. Devices were checked for handling damage after drying. The IDA was examined for shorts visually using a microscope; the integrity of the connection between copper lead wires and their contact pads was verified using the multimeter. Finally, the multimeter was connected across the IDA leads and the minimum stable resistance value was recorded.

3.4 Results and Discussion

Fabrication and modification of IDA electrodes. Gold slides were patterned using photolithography and then chemically etched to yield gold features on an insulating glass substrate as shown in Figure 3.1. The pattern consisted of two gold contact pads each extending toward one pole of a 2 x 2 mm IDA. An SEM micrograph of the fine features of the IDA is shown in Figure 3.2.

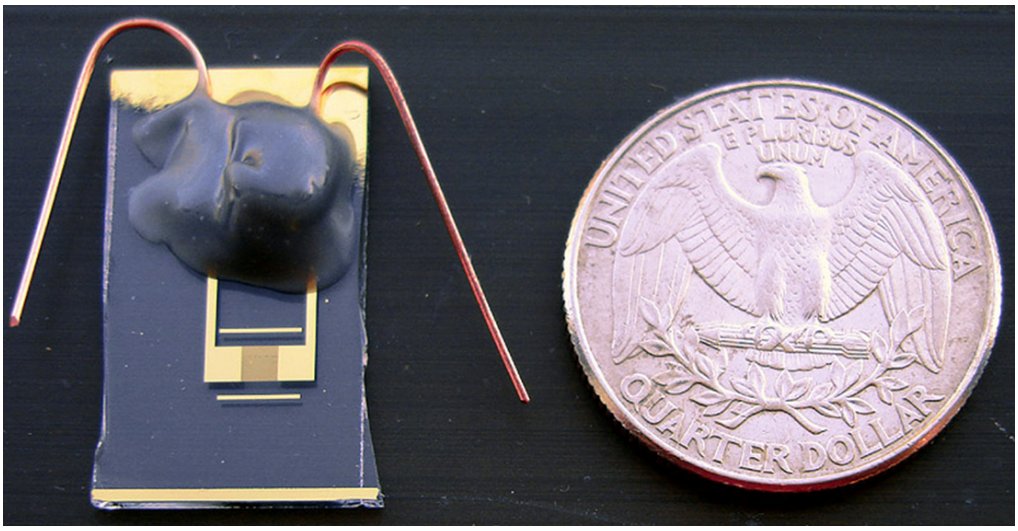

Figure 3.1. Photograph of a microfabricated IDA device with attached Cu lead wires referenced for size with a US quarter dollar coin.

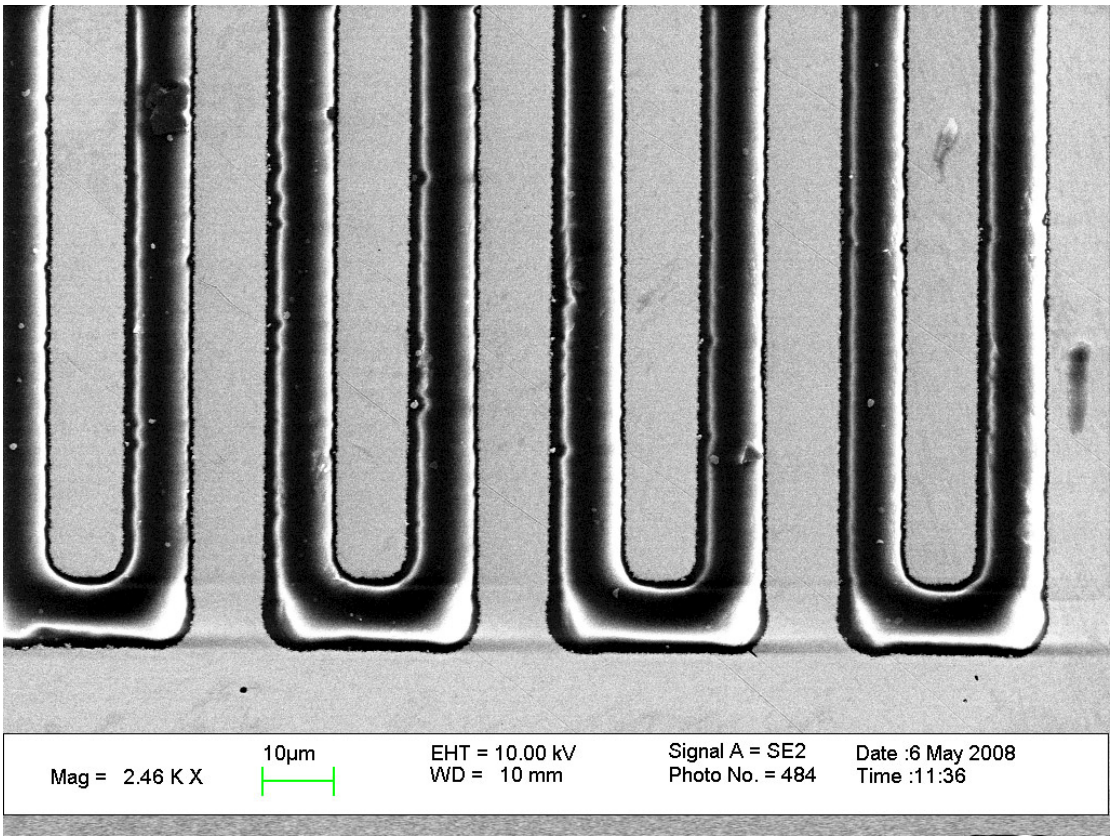

Figure 3.2. SEM image of the IDA at high magnification showing the 10 µm features of electrodes.

The electrodes of the IDA were positioned 10 µm apart and were connected to the multimeter using copper lead wires attached to contact pads. The electrodes were modified with a mixed monolayer of 5′ thiol-modified capture DNA and 1-hexane thiol before exposure to the target DNA solution. Hexane thiol was chosen to match the hexyl spacer present in the capture DNA, and to encourage silver deposition within the interstitial glass regions of the IDA.

Target detection and silver development. In a typical experiment, modified IDAs were exposed to a range of target DNA concentrations and then incubated for 2 h to facilitate hybridization. The target DNA was presented alone or as a "needle-in-a-haystack" of non-complementary, potentially interfering oligomers. After hybridization, streptavidin-modified AlkP was bound to the surface via its affinity for the 5′ biotin on the target. Enzyme was delivered in solution with Tween-20 and BSA to prevent non-specific adsorption. AlkP catalyzes the hydrolysis of the 2′ phosphate group of AsAP to yield reducing equivalents of AsA.

After incubating AsAP with the enzyme for 1 h, Tollen's reagent was added. Tollen's reagent has been used extensively as an indicator for aldehydes and in the Ag mirror reaction.[79] The solution-phase reaction between AsA and Ag^{+} leads to formation of Ag metal, which forms smooth deposits on the surface of the IDA. This two-step approach

involving, first, generation of reducing equivalents and, second, addition of the Ag^+ source, is different from previously reported procedures in which the Ag^+ source is introduced at the same time as the phosphorylated precursor. In the latter case, it has been found that the enzyme is partially deactivated by Ag during the assay.[60,62] This is not a concern in the system presented here, because the enzymatic hydrolysis reaction is complete before addition of Ag^+.

We observed that the film resulting from the reduction of Tollen's reagent was more conductive than when $AgNO_3$ or Ag_2SO_4 was used as the source of Ag (data not shown). Moreover, the inclusion of a warming step prior to development enhanced the adhesion of Ag onto the glass surface between the electrodes and thus increased conductivity. An additional 2 h in the humidity chamber was found to positively affect the conductivity of the deposit. Surface analysis by SEM in Figure 3.3 reveals two predominant types of features after biometallization with

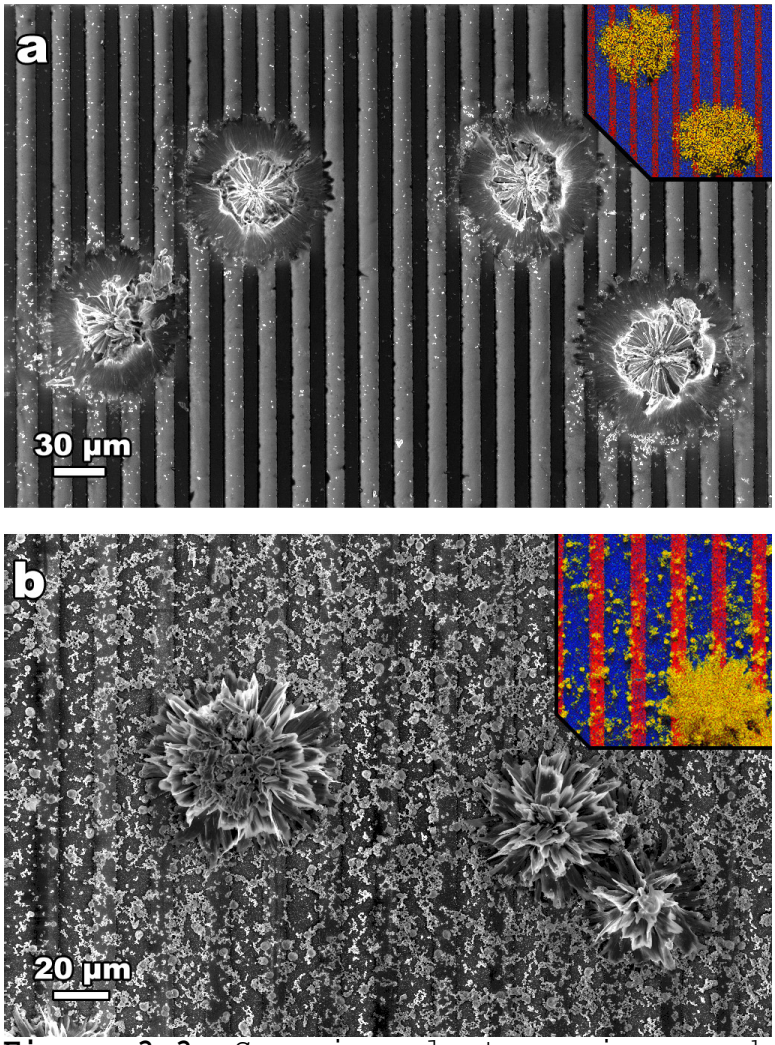

Figure 3.3. Scanning electron micrographs of IDAs exposed to 40 µL drops of solution containing (a) 100 aM and (b) 1 µM target DNA labeled with AP. The Au electrodes appear as dark, vertical lines, the glass interstitial regions are grey, and Ag deposits appear white. The insets are EDS maps showing the elemental composition of a portion of the micrographs. These maps indicate the locations of Ag (yellow), Au (red), and Si (blue).

Tollen's reagent: dendritic Ag deposits and hemispherical clusters consisting of radiating leaflets. The metallic dendrite structures spanning the gap between electrodes are responsible for the enhanced conductivity observed in the presence of the complementary target.

Dendritic growth of Ag is most apparent in Figure 3.3b, because this device was prepared for illustrative purposes using a very high concentration (1 μM) of enzyme-labeled target DNA. However, careful examination of the IDA shown in Figure 3.3a, which was prepared using 100 aM target, also reveals the presence of Ag deposits between electrodes. The insets shown in Figure 3.3 are element maps obtained using energy dispersive spectroscopy (EDS). These maps indicate the locations of Ag (yellow), Au (red), and Si (blue).

The relatively large, leafleted structures that dominate the micrographs in Figure 3.3 were consistently observed in target-containing assays, but they were also observed in many of the negative control experiments. Compositional analysis using EDS indicated that the clusters are mostly composed of Ag, but that they also contain a small percentage of carbon. Importantly, resistance measurements carried out on negative control devices on which these features were observed showed that they do not provide an electronically conductive pathway between the interdigitated electrodes. Therefore, they do not adversely impact the sensing experiments described in the next section. The composition and morphology of these clusters is

consistent with earlier studies of ascorbate-mediated Ag reduction in which silver ascorbate, an intermediate species, was isolated in the form of spherical particles several microns in diameter.[80]

By analogy to this previous study, and taking into account our finding that these features are not electronically conductive, we believe that at least the part of the clusters in contact with the interdigitated electrodes are composed of insulating silver ascorbate.

Target dose-response assays. The genosensor was evaluated at concentrations of target DNA between 1 fM and 1 aM. The oligonucleotide sequence complementary to the surface-confined probe was delivered to the device alone or mixed with non-complementary sequences, and each concentration was assayed using three to six replicate IDAs. Measured resistance values reflect the binary nature of this sensor, which yields either a positive or negative qualitative response. A positive response was defined as an IDA having a resistance <40 M (the maximum threshold for the multimeter). Data for the dose-response assays, with and without non-complementary DNA, are presented in Figure 3.4. The key result is that resistances for devices exposed to target DNA were found to be lower than 5 k whether or not non-complementary, unlabeled DNA was present in large excess (36.3 ng/mL).

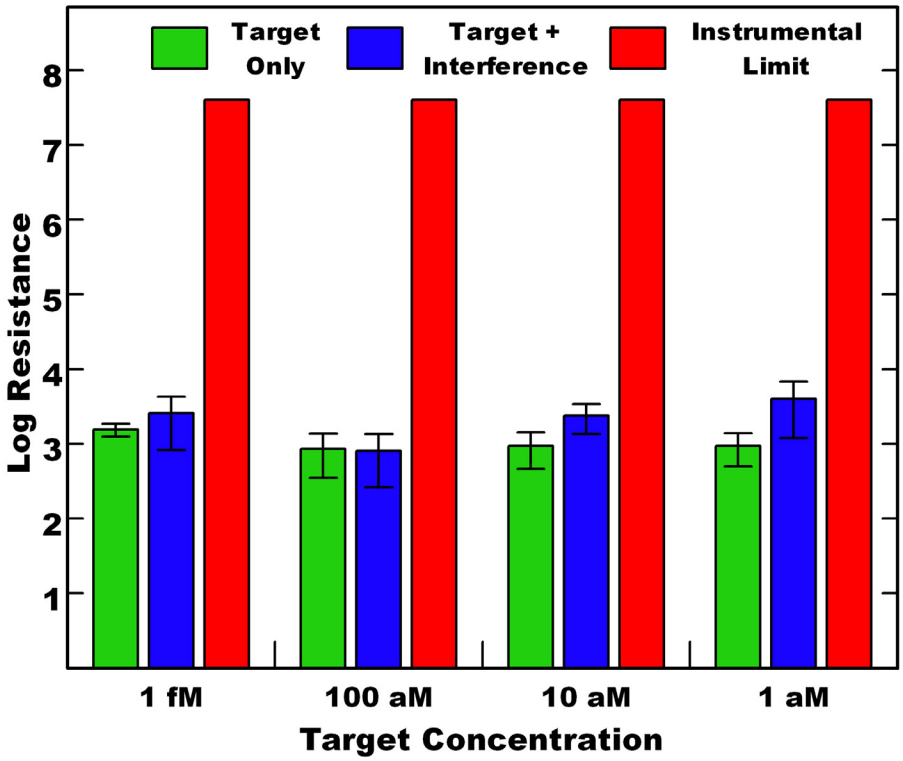

Figure 3.4. Resistance dose-response data for target DNA concentrations of 1 fM, 100 aM, 10 aM, 1 aM. The green bars represent the average resistance values for devices exposed to target DNA only (non-complementary DNA was excluded). The blue bars correspond to target DNA in the presence of 36.6 ng/mL of non-complementary, unlabeled DNA. The red bars represent the maximum threshold resistance of the multimeter (40 MΩ). Error bars represent one standard deviation from the average of three to six replicates. Prior to chemical modification, the IDA resistances of all control experiments referred to in the text exceeded 40 MΩ.

A series of control assays was performed to establish that the assay responds only to the labeled target. In all of the following control measurements, the IDA resistances were found to exceed 40 M : (1) naked IDAs and IDAs modified with probe DNA; (2) probe-modified IDAs exposed to complementary, biotinylated DNA before and after introduction of streptavidin-modified AlkP; (3) naked and probe-modified IDAs exposed to Tollen's reagent. Finally, and most importantly, when an IDA was modified with 5' thiol-modified DNA non-complementary to the target, exposed to enzyme-labeled target DNA at concentrations spanning the range represented in Figure 3.4, and subjected to the conditions required for biometallization, the IDA resistance was found to be >40 M .

3.5 Summary and Conclusions

The concentrations of target DNA used in these experiments are representative of EBV viral CNAs, and it is significant that such a simple sensor design can provide a qualitative genomic test without the need for PCR even in the presence of a large excess of non-complementary oligonucleotide sequences. In the most extreme case, represented by the 1 aM test solution (Figure 3.4), only 24 copies of the target DNA were delivered to the device. This sensor is sufficiently easy to use, and requires such minimal instrumentation, that one can imagine it being

implemented in remote, point-of-care applications where a simple "yes" or "no" response is required.

Chapter 4. A Self-Powered Sensor for Naked-Eye Detection of Serum Trypsin

4.1 Synopsis

In this chapter we describe a device for the detection of the proteolytic enzyme trypsin, which is a biomarker for pancreatitis. The sensor is self-powered, easy to use, and signals the presence of trypsin via a light-emitting diode (LED) that is visible to the unaided eye. Assay time is ~3 h and the limit of detection is 0.5 μg/mL, which is within the range required for detection of trypsin at levels signaling acute pancreatitis. The sensing mechanism relies on trypsin digestion of a gelled protein layer. Partial digestion of the protein layer permits hydroxide penetration and subsequent etching of an underlying Al membrane. Degradation of both the protein and Al layers exposes an underlying Mg anode and closes an electrochemical circuit that produces ~2.2 V. This is sufficient voltage to illuminate the LED. A logarithmic relationship is observed between the time required for LED illumination and trypsin concentration. The device is equally effective for trypsin dissolved in buffer or serum media.

4.2 Introduction

In this chapter we report a self-powered device for detection of trypsin in serum at pathological concentrations that uses a light-emitting diode (LED) to deliver a response

visible to the unaided eye. The assay is complete within ~3 h, and it provides quantitative results without requiring an external power source. The device, pictured in Figure 4.1, is an Mg//Fe^{3+} galvanic cell with protein and Al passivating layers blocking Mg oxidation at the anode. In the presence of trypsin and hydroxide, however, these passivating layers are etched, and this action connects the anode and cathode thereby illuminating the LED. However, in the absence of trypsin the protein passivating layer blocks LED illumination. We show dose-response assays using trypsin in both buffer and serum, and we report a relationship between the concentration of trypsin and the LED illumination time. The limit of detection is 0.5 µg/mL, even in the presence of the blood-borne proteins, sugars, and salts found in serum. The novelty of this single-use sensor arises from three factors.

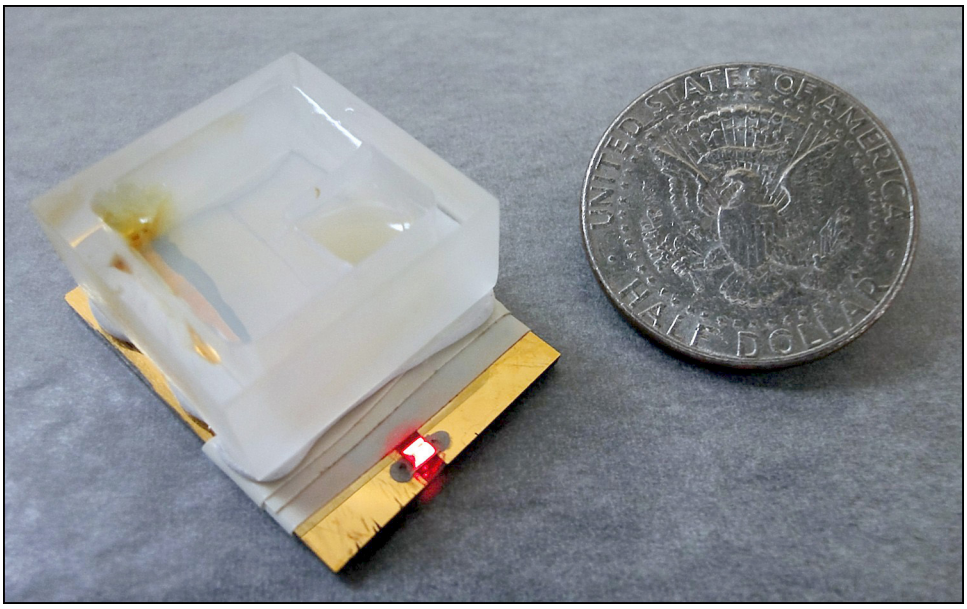

Figure 4.1. Photograph of the assembled Mg//Fe^{+3} cell discharging and emitting light from the LED. For size reference, the device is shown next to a US half dollar coin.

First, it is self powered by the $Mg//Fe^{3+}$ galvanic cell discussed earlier. Second, the presence of trypsin is reported by an LED, and therefore only the unaided eye is required for detection. Third, the device is simple to operate.

Trypsin is a digestive enzyme produced in the pancreas that cleaves proteins on the *c*-terminal side of arginine and lysine residues. It is most active under slightly alkaline conditions and in the presence of Ca^{2+}, Mg^{2+}, and Mn^{2+}.[81] Trypsin is formed initially as the proenzyme trypsinogen, which self-cleaves to yield the more active form as needed.[82] This self-regulating process can be adversely affected by pathologies, such as pancreatitis, which result in organ damage and release of enzyme into the blood. An immunoassay-based, quantitative study found healthy individuals to have a mean serum trypsin concentration of 0.25 ± 0.1 µg/mL, whereas acute pancreatitis patients exhibited a higher concentration of 1.4 ± 0.6 µg/mL.[26] Speed is a factor to consider when using trypsin as an indicator of pancreatitis. For example, a time-resolved ELISA study found that the serum trypsin concentration is at a maximum 24 h after the onset of symptoms, but it is decreased at 48 h and again at 72 h.[83] For diagnostic detection, a system must be sensitive to ~1 µg/mL enzyme, capable of distinguishing between small variations in concentration,

and sufficiently accessible so as to be implemented immediately after the appearance of pancreatic symptoms.

Ionescu et al. have published an indirect electrochemical method for trypsin detection using a catalyst-modified Pt disk electrode that generates an electroactive species that can be detected by cyclic voltammetry.[27] In this study, electrodes were modified with electropolymerized glucose oxidase (GOx) and coated with a layer of gelatin. When immersed in a solution containing trypsin (9380 U/mg) and glucose, the enzyme digested the gelatin layer, and GOx converted glucose to electroactive peroxide.

The sensing device described here relies on an LED to signal the onset of an electrochemical reaction.[23] Previous electrochemical studies have used LEDs to report the passage of current in a battery and as a component in more complex circuits to interrogate and quantify electroactive species under external potential control.[23-24] The LED used here has a minimum turn-on voltage of ~1.7 V and is self-powered by the two half cells comprising the sensor. Specifically, Mg oxidation and Fe^{3+} reduction yield an observed cell voltage of ~2.2 V. Self-powered sensors have been demonstrated previously. Biofuel cells developed by Willner, Katz and Minteer use anodes modified with enzymes or mitochondria to detect sugars[84] and nitroaromatics[85], respectively. This work is distinct from these previous studies in that passive surface modifications overly a reactive metal anode.

In this chapter, we present a method for the indirect detection of trypsin in serum. The limit of detection is ~0.5 µg/mL, which is sufficiently low for detection of pathological conditions. The device provides a logarithmic response that spans more than two orders of magnitude in trypsin concentration, regardless of whether the analyte is present in buffer or serum. Detection is achieved with just the unaided eye within 3 h of analyte injection. Finally, the device is fully self-powered and therefore appropriate for many point-of-care applications, including those in remote locations.

4.3 Experimental Section

Chemicals and materials. Trypsin from porcine pancreas, Type IX; gelatin, Type A, 300 bloom electrophoresis grade from porcine skin, heat-inactivated and sterile filtered equine serum, and calcium acetate monohydrate (> 99%), henceforth referred to as CaAc, were purchased from Sigma (St. Louis, MO). Genetic-analysis grade agarose and N_a-*p*-tosyl-L-arginine methyl ester (TAME) hydrochloride were obtained from Thermo Fisher Scientific (Waltham, MA). BiPRO whey protein isolate, henceforth referred to as WPI, was purchased from Davisco Foods International (LaSueur, MN). Magnesium alloy AZ31B was obtained in 1 mm-thick, flat sheets from A1 Alloys (San Diego, CA). This alloy is ~95% Mg and has electrochemical properties similar to those of pure Mg. Glass microscope

slides coated with Au (100 nm) and having a Cr adhesion layer (5 nm) were obtained from EMF Corporation (Ithaca, NY). The LEDs (part no. SML-LX1206SIC-TR, Lumex, Palatine, IL) were surface-mounted red emitters (λ = 636 nm). Their size was 3.2 mm x 1.6 mm, and they had a typical forward bias of 2.0 V and an axial luminous intensity of 70 mcd at a typical current of 20 mA. Double-sided conductive Cu tape and conductive glue (Silver Adhesive 503) were purchased from Electron Microscopy Sciences (Hatfield, PA). Electroplating tape and Scotch-brand adhesive putty were purchased from 3M (St. Paul, MN). The Al foil used in this chapter was Reynolds Wrap commercial kitchen foil from Reynolds Food Packaging (Richmond, VA). Aqueous solutions were prepared using 18 M -cm water from a Millipore Milli-Q system (Billerica, MA).

Instrumentation. Magnesium strips were cleaned and smoothed using a digital rotary tool (Model 398, Dremel, Racine, WI). Device integrity was verified at several points during assembly using a multimeter (Fluke 79 Series II) and a DC power supply (Model No. HP3620A, Hewlett-Packard, Palo Alto, CA). Enzyme activity assays were monitored using a photodiode array UV vis spectrometer (Model No. 8453, Agilent Technologies, Santa Clara, CA).

Cell assembly. Components of the sensing platform are shown in Scheme 4.1. The device components are labeled and displaced vertically with respect to order of assembly.

Scheme 4.1

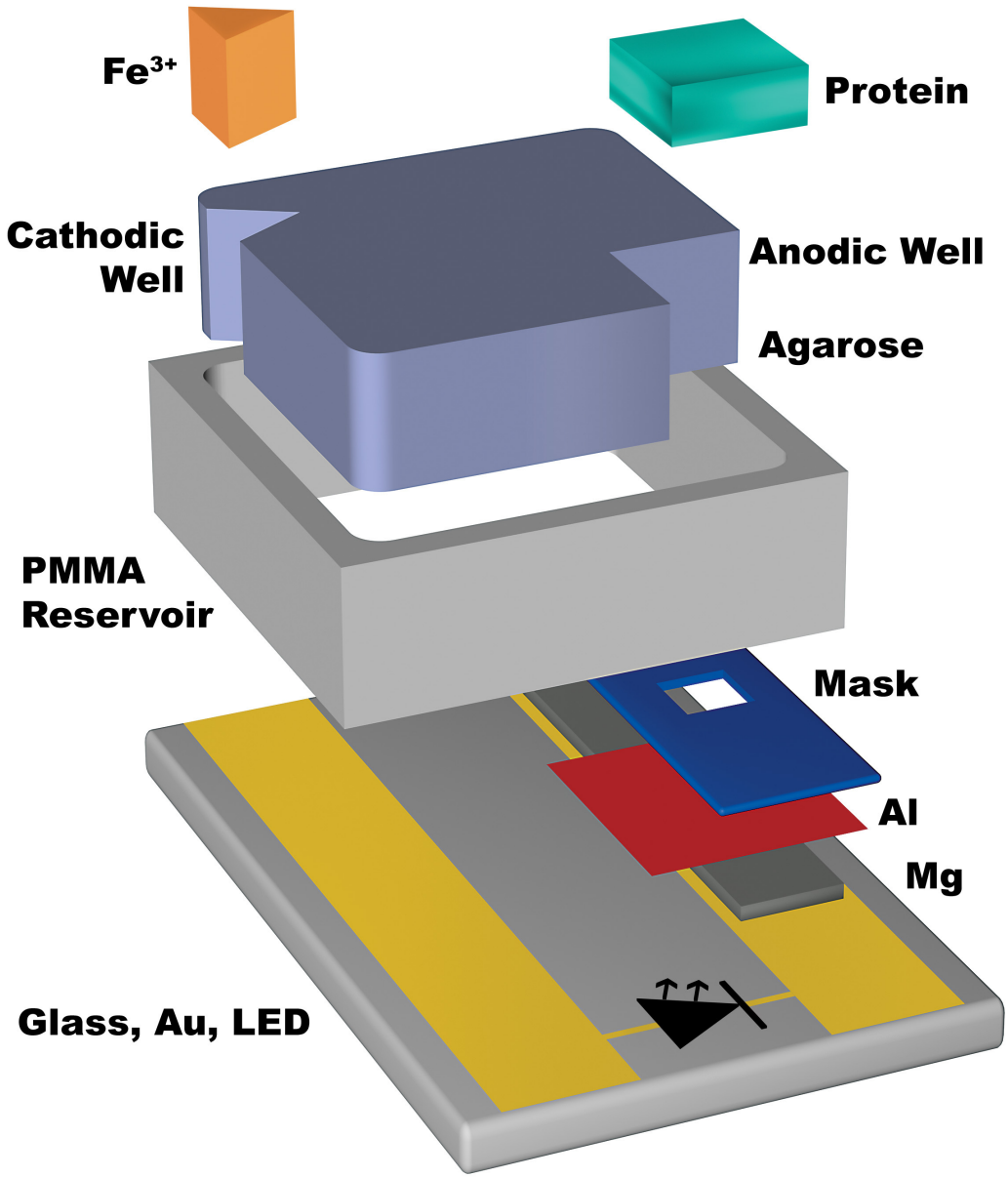
Fe3+
Protein
Cathodic Well
Anodic Well
Agarose
PMMA Reservoir
Mask
Al
Mg
Glass, Au, LED

Specifically, the Au-coated glass slides were cut into 4.0 cm x 2.5 cm pieces and patterned, using an etch-resistant ink (Sharpie permanent marker, Sanford LP, Oak Brook, IL), so as to provide two Au electrodes: a cathode and a contact pad to support the Mg anode. The exposed Au was removed by immersing the slide in a solution containing 8% KI and 2% I_2 (both w/v). After rinsing with water, the Cr layer was removed using a solution containing 9% $(NH_4)_2Ce(NO_3)_6$ (w/v) in 6% $HClO_4$ (v/v). The slides were rinsed with water, dried, soaked in acetone, absolute ethanol, and finally dried again. The surface-mount LED was connected to the Au electrodes using conductive Ag adhesive. Electrical connections were evaluated by applying 2.0 V to the Au electrodes to ensure illumination of the LED. Devices fitted with LEDs exhibiting high brightness were retained, and the LED was secured to the glass slide using an insulating epoxy.

The Mg strip was covered with commercial Al foil. The Al foil was cut into 1.0 cm^2 pieces taking care to avoid punctures. Tape was used to secure the foil over the Mg, and then both metals were completely covered with electroplating tape except for a 5.1 ± 0.5 mm^2 window centered in the middle of the Al foil. A poly(methylmethacrylate) (PMMA) reservoir was cut into a square ring from a 1.3 cm-thick sheet, and it was secured to the substrate using a thin bead of contact-adhesive putty. A salt bridge mixture was prepared by heating a solution of 3% (w/v) agarose in 2 M

KCl on a 150 °C hotplate with stirring until the solution was boiling and clear. The molten agarose was poured into the PMMA reservoir and allowed to solidify. Finally, a small triangular cathodic well and a larger square anodic well were excised from the agarose salt bridge using a scalpel. To ensure device-to-device reproducibility, the anodic well was cut using a metal guide to a uniform area of 0.8 ± 0.2 cm^2.

Gelatin and WPI were selected as the components of the protein layer. Protein solutions were prepared in 0.7 M HEPES buffer at pH 7.55. The concentrations of the proteins were individually optimized for buffer and serum. For buffer-based assays, the protein solution contained 5% gelatin and 10% WPI (both w/v). For detection of trypsin in serum, the protein solution contained 6% gelatin and 9% WPI (both w/v). The protein powders were added to solution in conical tubes and dispersed using a vortex mixer. The tubes were placed in a sonicating water bath at 60 °C for 15 min to dissolve the proteins and defoam the solution. During the preparation and handling of the protein solutions, it was important to limit bubble formation to avoid pinholes that could lead to premature etching of the Al foil. After sonication, the molten protein was aliquoted and stored at 4 °C until needed. Just prior to running an assay, these aliquots were placed in a sonicating bath at 60 °C for 2 min, and then 250 µL of the solution were added to the anodic well of each device. Cathodic wells were filled with

50 µL of 0.2 M $FeCl_3$. The devices were then chilled at 4 °C for 30 min to gel the protein. Devices were inspected before use, and those having a smooth, bubble-free protein layer and a non-illuminated LED were retained for assays.

Trypsin assays. The assays were carried out using 100.0 µL volumes of buffer or serum with or without added trypsin. The evaluation of the activity of trypsin is described in the Supporting Information. Stock trypsin solutions were prepared daily at a concentration of 10.0 mg/mL in either buffer or serum and diluted to concentrations ranging from 0.50 µg/mL to 100 µg/mL. Buffer trials used trypsin in 46 mM, pH 8.0 TRIS containing 11.5 mM CaAc. For serum trials, trypsin was diluted into 100.0 µL of equine serum having a native pH of 7.9, and then an additional 13.0 µL of 0.115 M CaAc were added. Negative control assays used 100.0 µL volumes of buffer or serum, with an additional 13.0 µL of 0.115 M CaAc added to the serum assays. The test solution was added to the cathodic well of each device, which was then placed in a closed Petri dish inside an air incubator at 26 ± 1 °C and left for 2 h. During incubation, the incubator maintained a constant temperature compatible with the stability of the protein layer and the activity of trypsin while ensuring uniform conditions between assays. After incubation, an additional 50.0 µL of 0.20 M Fe^{3+} solution was added to the cathodic well to compensate for solution sorbed into the gel during incubation. Devices having an illuminated LED at this stage

were discarded. Finally, the Al dissolution process was initiated by adding 300 µL of 1.0 M NaOH to the anodic well. The time between hydroxide addition and LED illumination was recorded.

4.4 Results and Discussion

Device overview. This trypsin sensor is designed around an electrochemical cell comprised of two half cells in which Fe^{3+} is reduced and Mg is oxidized. Prior to adding the analyte, the two half cells are prevented from discharging by the presence of Al and protein barrier layers positioned above the Mg anode (Scheme 1). However, when trypsin is added to the anodic well, it degrades the protein layer. Subsequent addition of hydroxide etches the Al passivating layer,[86] and this exposes the Mg anode to the KCl-impregnated agarose salt bridge.[87] Now the two half cells are in electrochemical contact, and sufficient voltage is provided to illuminate an LED. Hence, the LED signals the presence of trypsin. If the added analyte does not contain trypsin, then the protein layer remains intact and retards transport of hydroxide to the Al layer. Therefore, the electrochemical circuit remains open and LED illumination is prevented. More detailed information about device operation is provided later.

Dose-response assays. Dose-response assays were carried out for trypsin in buffer and serum. The assay was initially optimized using trypsin in buffer, and then the

protein gel was re-optimized for detection of trypsin in serum. Specifically, the amount of gelatin was increased from 5% to 6% and WPI was concomitantly decreased to keep the total amount of protein constant. The additional gelatin used for the serum assays prevented delamination of the protein layer from the Al, which was observed only when serum media was used.

Data from the trypsin assay in buffer and serum are shown in Figure 4.2. The average time between addition of hydroxide and LED illumination time for 3-5 different devices is plotted against the different trypsin concentrations and a trypsin-free negative control. The error bars represent one standard deviation from the mean. It is important to note that even for the lowest trypsin concentration (0.50 µg/mL) the error bars do not overlap with the negative control assay. The inset in Figure 4.2 shows that there is a linear relationship between the mean time for LED illumination and the logarithm of the trypsin concentration. The R^2 values for the buffer and serum fits are 0.96 and 0.99, respectively. Because the inset plot is concerned with the response of the system to changes in trypsin concentration, the trypsin-free, negative control data are not included.

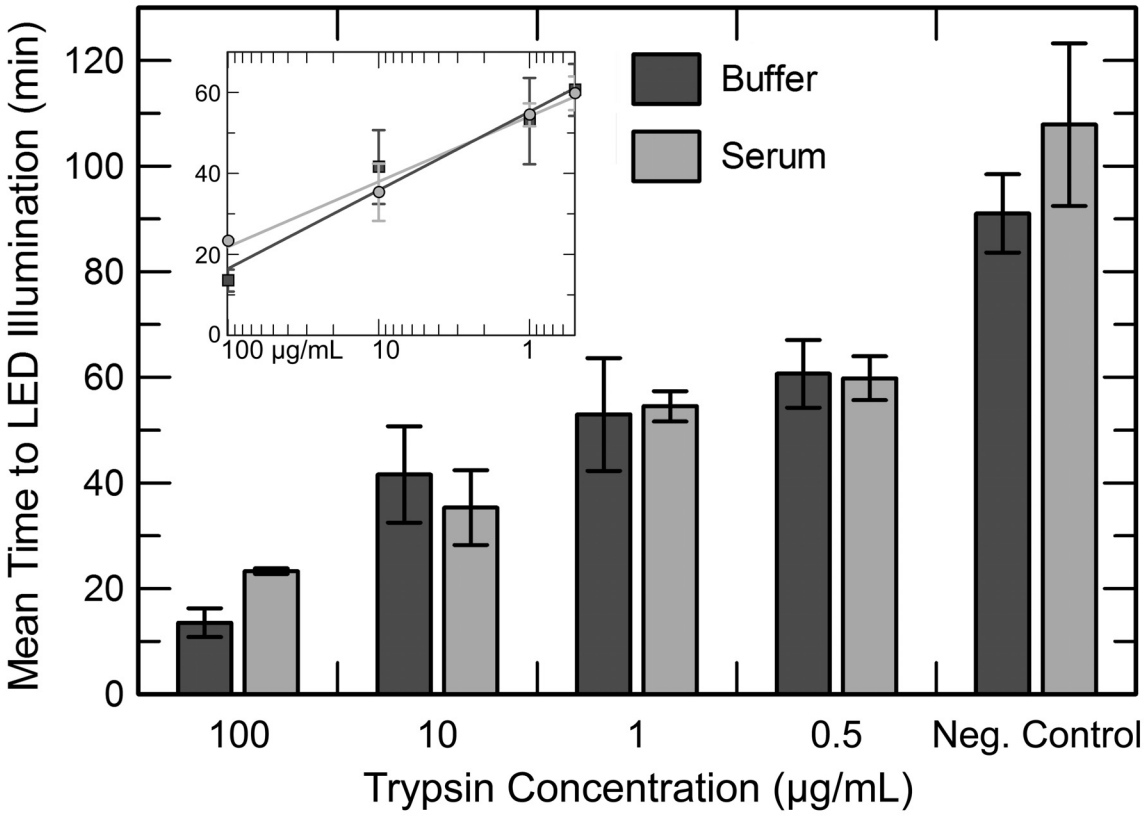

Figure 4.2. A histogram correlating the average time between addition of hydroxide and illumination of the LED to the concentration of trypsin present in buffer or serum. The negative control was obtained for a trypsin-free sample. The inset is a semi-log, least-squares plot correlating the average illumination time to the concentration of trypsin. Error bars represent one standard deviation from the average of data obtained for 3-5 independently prepared sensors.

Control Assays. Control assays confirmed that degradation of the gelatin/WPI composite protein layer depends on the presence of trypsin and that the protein layer itself does not degrade Al on the time scale relevant to this study. For the dose-response study, negative control devices exposed only to solvent (buffer or serum) were tested alongside devices exposed to trypsin. Positive control devices lacking a protein layer usually illuminated within 1 min after exposure to hydroxide.

Role of the protein gel and Al barrier layers. A diagram illustrating the roles of the protein and Al barrier layers is shown in Scheme 4.2. In Frame *a*, the protein gel layer is exposed to a solution containing trypsin. Trypsin partially digests the protein layer, which renders it more permeable to hydroxide than the native gel. After trypsin digestion for 2 h, hydroxide is introduced into the anodic well. Frame *b* shows that hydroxide penetrates the digested protein layer and partially dissolves the Al layer to expose the Mg strip. This closes the electrical circuit and results in LED illumination. However, in the absence of trypsin digestion (Frame *c*), migration of hydroxide through the gel layer is slowed and therefore LED illumination is delayed.

Scheme 4.2

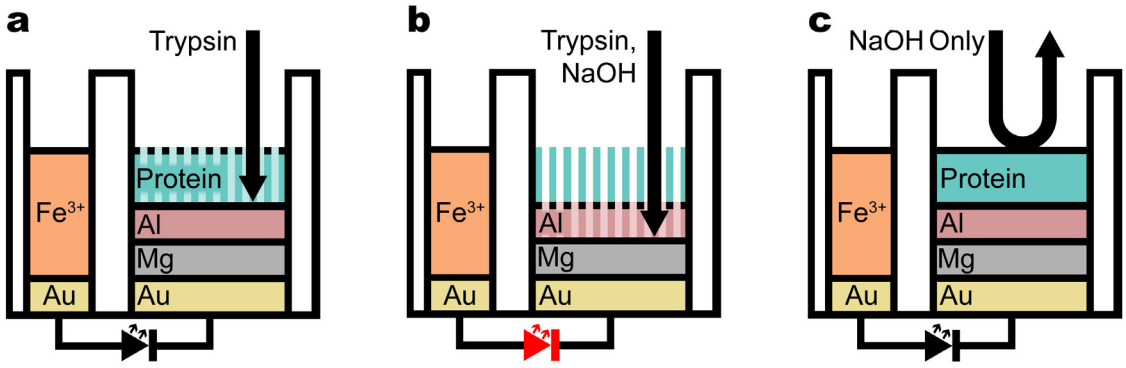
a
Trypsin
Protein
Fe3+
Al
Mg
Au
Au
b
Trypsin,
NaOH
Fe3+
Al
Mg
Au
Au
c
NaOH Only
Protein
Fe3+
Al
Mg
Au
Au

The difference in illumination times arises from the properties of the two proteins used in the barrier layer as illustrated in Figure 4.3 Gelatin gels by heat-induced (> 50 °C)[28] denaturation followed by hydrogen-bond-driven coalescence.[88] However, gelatin is unstable in the presence of hydroxide, so WPI is added to improve its tolerance to basic conditions. WPI stabilizes the gel under basic conditions, because it denatures at alkaline pH thereby exposing buried cysteine residues that can polymerize via disulfide bonding[34,88-89] to form a rigid, proteinaceous solid.[34,89]

Once polymerized, a WPI-containing gel is hydroxide resistant unless it has previously been treated with trypsin to degrade the gelatin component. In this latter case, hydroxide moves through the protein layer, and then encounters and degrades the Al barrier. In the absence of trypsin, the added base polymerizes WPI and rigidifies the gel thereby increasing the time required for base attack on the protective Al membrane. The key point is that the rate of hydroxide transport through the gel depends on the concentration of trypsin (Figure 4.2).

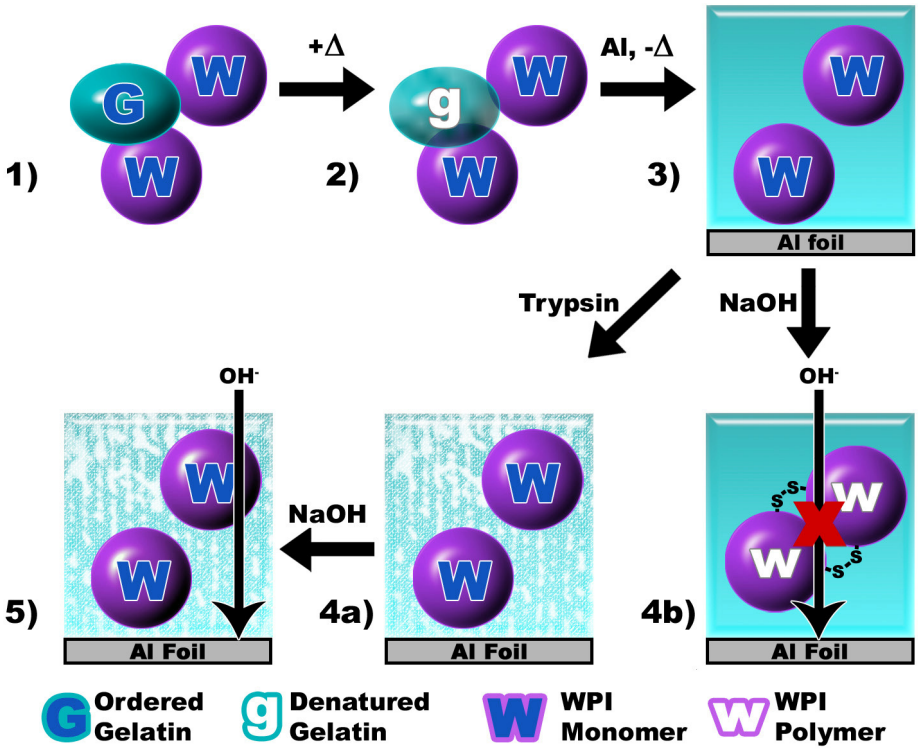

Figure 4.3. Mechanism for the enzyme-labile and hydroxide-resistant protein layer. In step 1, gelatin is combined with WPI in solution, and heated in step 2 to denature only the gelatin. The molten solution is applied to the Al foil layer and cooled, forming gelatin gel in step 3. If exposed to trypsin, as in step 4a, the gel is digested to allow hydroxide to reach the Al layer as in step 5. Gels not exposed only to hydroxide, shown in 4b, undergo WPI gelation that consumes and delays diffusion to the Al layer.

4.5 Summary and Conclusions

In this chapter we have described a self-powered trypsin sensor that is easy to use, detects trypsin at pathological concentrations in serum, and signals detection with an LED in ~3 h. The range of trypsin concentrations that can be quantitated includes those that are characteristic of acute pancreatitis. The discharge of the galvanic cell is gated by the two-component protein gel. That is, in the presence of trypsin the gel is degraded and this results in faster transport of hydroxide and subsequent corrosion of the underlying Al barrier. In the absence of trypsin, however, base polymerizes the WPI component of the protein layer and increases the time required for hydroxide to etch the Al barrier. Another important aspect of this sensor is that it is self-powered. In essence, the device is a battery having a trypsin-selective switch that closes the circuit between the anode and cathode. The sensor works equally well in buffer or serum, demonstrating the resiliency of this method to the endogenous proteins, sugars, and salts present in real biological fluids.

Chapter 5. Stabilization of Alkaline Phosphatase with $Au@Ag_2O$ Nanoparticles

5.1 Synopsis

In this chapter we report that a conductive $Au@Ag_2O$ nanoparticle structure significantly enhances the stability of alkaline phosphatase (AlkP) in the presence of the inhibitors urea and L-phenylalanine (Phe). The enzyme/nanoparticle construct is prepared by associating the enzyme with citrate-capped Au particles, and then adding Ag^+. UV-vis and XPS spectroscopy, and transmission electron microscopy, confirm the core@shell structure. AlkP activity was quantified in the presence and absence of the two inhibitors using a time-resolved colorimetric assay. The results indicate that 21% of the initial active AlkP is incorporated into the nanoparticle structure. More importantly, however, the $Au@Ag_2O$ core@shell host reduces the inhibitory effect of urea and Phe by factors ranging from 3-12, depending on the inhibitor and its concentration, compared to the wild-type enzyme.

5.2 Introduction

In this chapter we describe the stabilization of alkaline phosphatase (AlkP) against organic inhibitors by core@shell colloidal nanoparticles (NPs). These composites are prepared by combining AlkP and an Au colloid solution with Ag^+. This

results in agglomerated particles having an Ag_2O shell (AlkP-Au@Ag_2O), which stabilizes and protects the enzyme against inhibitors that would otherwise greatly reduce its activity. This finding is significant, because many applications are carried out under less-than-optimal conditions for enzyme functionality.

AlkP is a common enzyme that has previously been isolated and characterized.[6,47] The wild type (WT) bovine intestinal isoform is an effective catalyst for the hydrolysis of phosphate groups present on a wide variety of substrates, has an approximate molecular weight of 60 kDa, and exhibits optimal activity under moderately basic conditions (pH 9-10).[6] AlkP is often integrated into analytical assays and sensing schemes owing to its ease of handling and high catalytic activity.[47,90] To improve the stability of AlkP and other enzymes used for applications like biosensing, there has been interest in encapsulating them within more rugged host materials. For example, Braun et al. encapsulated AlkP in a bulk sol-gel matrix that was subsequently pulverized and used as column packing material. AlkP in this matrix exhibited a 15% greater tolerance for incubation at 70 °C relative to free AlkP in solution.[40] Smith et al. examined the activity of horseradish peroxidase (HRP) in sol-gel monoliths, coatings, and pulverized powders and reported that the powder form of HRP was active and reusable.[41] These results are also important as they show sol-gel protein entrapment is not exclusive to AlkP. Sol-

gels have also been used to protect proteins against drying. For example, Li et al. entrapped a fluorescent protein inside a sol-gel slab and reported that the protein remained fluorescent after lyophilization and rehydration.[91] A loss of the fluorescence signal would indicate changes in the protein structure. The key point common to all of these examples is that sol-gel hosts have been shown to stabilize some proteins against common degradative practices including heating, aging, and drying.

The previously discussed sol-gel materials entrap enzymes within a network of pores.[40] Alternatively, individual enzymes can be stabilized by other types of coatings that are directly attached to the enzyme. For example, Kim et al. modified surface amines on chymotrypsin with alkyl silanols to yield porous silicate gels around the enzyme.[44] This treatment was shown to extend the active lifetime of the enzyme in solution. Thiol groups were used in a similar way to reduce Au^{3+} onto α-amylase and form ~30 nm NPs that retained amylase activity. Like sol-gels, the Au shell was determined to be porous by screening for amylase activity using substrates with different molecular weights. HRP has been isolated within porous, hollow nanoshells.[92] In this experiment, AgCl-entrapped HRP colloid was prepared inside reverse micelles. $HAuCl_4$ and a reducing agent were phase-partitioned sequentially into the micelles, and after purification of the particles the AgCl was removed with

ammonia to leave active HRP inside an Au shell. Ben-Knaz and Avnir reported that acid phosphatase could be stabilized inside a metal powder by incubating the enzyme in solutions of Ag^{+} or Au^{3+} and adding Zn^{0} as a reducing agent.[46]

In the present manuscript we report the stabilization of AlkP against the inhibitory chemicals urea and L-phenylalanine (Phe) using composite NPs. We characterized these AlkP-Au@Ag_2O NPs using transmission electron microscopy (TEM), UV-vis spectroscopy, X-ray photoelectron spectroscopy (XPS), and energy dispersive spectroscopy (EDS). The results indicate that AlkP strongly associates with Au colloids and that the addition of Ag^{+} to the enzyme-NP conjugate yields a Ag_2O shell. AlkP activity was quantified using a time-resolved colorimetric assay, and the data indicate that ~21% of the active enzyme initially present is associated with the AlkP-Au@Ag_2O composite. Finally, the activity of free AlkP was compared to that of AlkP-Au@Ag_2O in the presence of two inhibitors. Under otherwise identical conditions, AlkP-Au@Ag_2O was at least three times more active, which demonstrates the stabilizing effect of the Ag_2O shell. Two key advantages of the method described here, compared to previous literature reports, are that this approach uses a one-pot synthesis and the time required to stabilize the enzyme is less than one day.

5.3 Experimental

Chemicals and materials. Citrate-capped Au colloids with a nominal diameter of 5 nm, Silver Enhancer Solution A (henceforth referred to as Ag^+ solution), *p*-nitrophenol phosphate disodium salt hexahydrate, enzymology grade (pNPP); and L-phenylalanine (Phe), USP, were purchased from Sigma (St. Louis, MO). Calf intestinal AlkP solution was purchased from New England Biolabs, Inc. (Ipswich, MA). Urea, ACS grade, was purchased from Thermo Fisher Scientific (Waltham, MA). Diethanolamine, 99%, was obtained from Alfa Aesar (Ward Hill, MA). Amicon Ultra-4 centrifugal filter sets having a 100 kDa molecular weight cut off (MWCO) were obtained from Millipore (Billerica, MA). Carbon-coated Cu TEM grids, 400 mesh, were purchased from Electron Microscopy Sciences (Hatfield, PA). Disposable UV-transmissive cuvettes with a 1.0 cm path length were purchased from BRAND GmbH (Wertheim, Germany). All chemicals were used as received. Aqueous solutions were prepared using 18 MΩ·cm Milli-Q water (Millipore).

Synthesis of AlkP and NP solutions. These solutions were prepared using a 1.0 M glycine solution adjusted to pH 9.2. Solutions were prepared in capped glass vials at an ambient temperature of 21 ± 2 °C. Four species were characterized in this chapter, and they are identified using the following notations: AlkP, Au@Ag_2O, AlkP-Au, and AlkP-Au@Ag_2O. AlkP solutions of enzyme alone were prepared by

combining 4.0 µL of AlkP with 1.35 mL of the glycine solution, and then stirring for ~18 h. Au@Ag_2O, which is a NP species having an Au core and an Ag_2O shell (but no enzyme), was prepared by combining 1.0 mL of Au colloid solution and 0.35 mL of glycine, stirring for ~18 h, and then adding 50.0 µL of Ag^+ solution. The mixture was then stirred for an additional 2.0 h. AlkP-Au, which is an enzyme-Au colloid conjugate, was prepared by combining 1.0 mL of Au colloid solution, 0.35 mL of glycine, 4.0 µL of AlkP, and then stirring for ~18 h. AlkP-Au@Ag_2O was prepared as described for AlkP-Au, with the additional steps of adding 50.0 µL of Ag^+ solution followed by stirring for 2.0 h. All species were isolated by filtration in which the crude solution was transferred to the reservoir of a MWCO tube and centrifuged for 10.0 min at 3000 x g. The filtrate was collected, and the pellet was resuspended with 1.0 mL of water and centrifuged again for 10.0 min at 3000 x g. The eluted liquid, hereafter referred to as the wash, was pooled with the initial filtrate and retained for analysis. The pellet was re-suspended with 1.0 mL of water and transferred to a microcentrifuge tube for subsequent analysis.

Characterization. UV-vis spectra of filtered and desalted solutions of Au colloid, Au@Ag_2O, AlkP-Au, and AlkP-Au@Ag_2O were obtained using a Hewlett-Packard HP8453 spectrometer (Santa Clara, CA). TEM micrographs of AlkP-Au, Au@Ag_2O, and AlkP-Au@Ag_2O were collected on a FEI TECNAI G2 F20 X-TWIN instrument (Hillsboro, OR). Grids were prepared

by drop casting 5.0 µL of each solution onto a TEM grid and drying overnight in a vacuum desiccator. Element maps and scanning/transmission electron microscope (STEM) images of AlkP-Au@Ag_2O were captured on a Hitachi S5500 with a Bruker Quantax 4010 EDS detector operating at 30 kV in bright-field mode (Pleasanton, CA and Billerica, MA, respectively). TEM Grids for STEM and EDS were prepared as for TEM, but included an extra drying step where the grids were lyophilized for 48 h. XPS analysis was carried out using a Kratos Axis Ultra spectrometer having an Al Kα filament (Chestnut Ridge, NY). XPS spectra were collected for Au colloid, Au@Ag_2O, AlkP-Au, AlkP-Au@Ag_2O, and WT AlkP. Samples of Au colloid, Au@Ag_2O, AlkP-Au, and AlkP-Au@Ag_2O were prepared by drop casting 20 µL volumes onto sections of Si wafer and drying for 24 h in a vacuum desiccator. WT AlkP specimens were prepared by dropcasting 10 µL of AlkP solution onto Au-coated glass and drying for 24 h in a vacuum desiccator. Spectra were collected at a pass energy of 20 eV with a step size of 0.1 eV for individual element scans. Sample charging was compensated by referencing the observed C 1s C-C peak to 284.5 eV.[58]

AlkP activity assay. Time-resolved colorimetric assays were used to measure the active quantity of AlkP in diethanolamine (DEA) units (U) for WT AlkP, AlkP-Au, Au@Ag_2O, and AlkP-Au@Ag_2O. One AlkP DEA U is defined as the amount of enzyme required to hydrolyze 1 micromole of pNPP

per minute. Activity testing was performed for each sample on the pooled filtrate and wash fraction, and on the resuspended pellet fraction. The activity assay method was adapted from literature reports.[48,93] Assays were carried out in a buffer containing 1.0 M DEA and 1.0 mM $MgSO_4$ adjusted to pH 9.8 with H_2SO_4. Briefly, 1.7 mL of buffer, 20.0 µL of the test solution and 0.10 mL of 150 mM pNPP were added to a cuvette and mixed by repetitive pipetting. The absorbance at 405 nm (A_{405}) was recorded at 0.50 min intervals for 6.0 min. A least-squares fit was applied to the linear data to obtain the change in A_{405} as a function of time (ΔA_{405} min^{-1}). The activity in U was then calculated from the ΔA_{405} min^{-1} value as described in the literature.[93] Between 3 and 5 replicates for each analyte were assayed.

Inhibition assays were performed on solutions of WT AlkP, AlkP-Au, and AlkP-Au@Ag_2O. For these assays, either urea or Phe was added to the DEA solution prior to testing. AlkP activity was measured at urea concentrations of 2.5 or 5.0 M, and Phe concentrations of 10.0 or 50.0 mM; the UV-vis blank contained DEA buffer, inhibitor at an appropriate concentration, and pNPP. The inhibitor assays were then performed using the same procedure as the activity assays, with the added step of allowing the test solution and inhibitor-containing DEA solution to incubate for 30.0 min prior to pNPP addition and UV-vis analysis. Different concentrations of enzyme were necessarily used for the WT

AlkP, AlkP-Au, and AlkP-Au@Ag_2O assays, and therefore the results were normalized as discussed later.

5.4 Results and Discussion

As discussed in detail in the Experimental Section, AlkP-Au@Ag_2O colloids were prepared in three steps. First, AlkP was mixed with citrate-capped Au colloid and glycine solutions. Glycine is compatible with AlkP activity[6] without adversely affecting the Au colloids.[94] Second, a Ag^+ solution was added to this mixture. After incubation, the resulting material was purified and characterized. Additional information about the synthesis of the other NP species discussed in this report is provided in the Experimental Section.

TEM micrographs of Au@Ag_2O and AlkP-Au@Ag_2O are shown in Figure 5.1. In Figure 5.1a, two populations of Au@Ag_2O particles are evident: discrete particles and small aggregates. The core@shell nature of these materials is suggested by the contrast difference between the dark centers and lighter periphery. The contrast difference is more apparent in the higher magnification image provided in the inset. In Figure 5.1b, two populations of AlkP-Au@Ag_2O are also observed: small spherical particles and larger agglomerates. The smaller particles resemble the Au@Ag_2O NPs in Frame a.

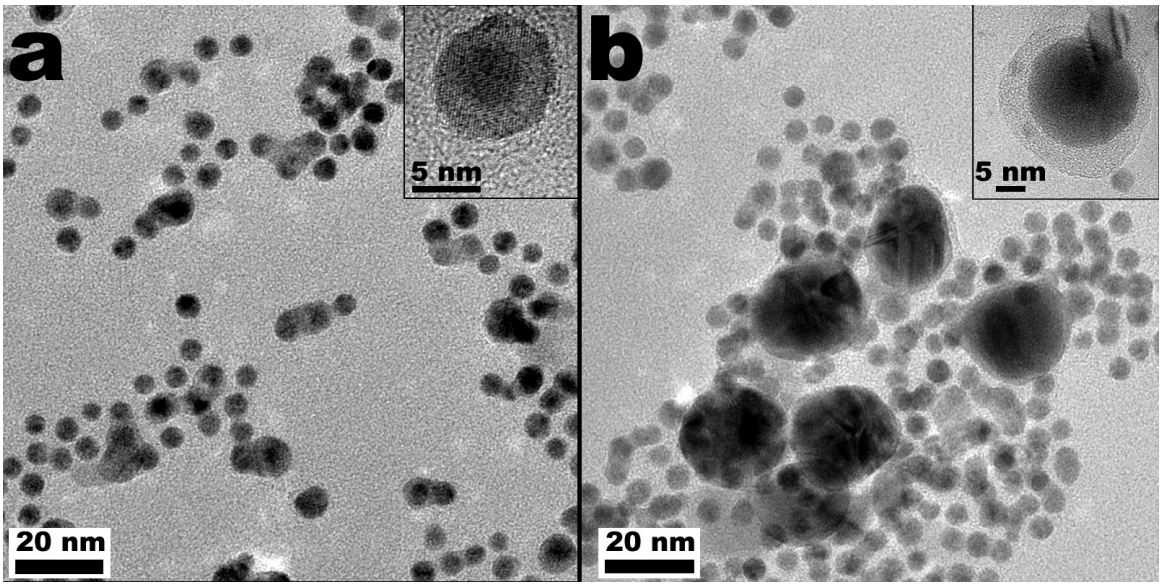

Figure 5.1. TEM micrographs of (a) Au@Ag_2O and (b) AlkP-Au@Ag_2O. Two particle populations are present for each species. The insets show higher magnification images of individual particles and highlight the core@shell morphology.

The larger agglomerates were observed consistently in AlkP-Au@Ag_2O preparations, but they were not present in Au@Ag_2O samples. The inset of Figure 5.1b shows a high magnification image of a large AlkP-Au@Ag_2O agglomerate, and it is apparent that these materials also have a core@shell structure. TEM analysis of AlkP-Au, Figure 5.2, indicates well-dispersed, unagglomerated particles exhibiting uniform contrast. On the basis of the morphology of the large AlkP-Au@Ag_2O agglomerates and their presence only in the AlkP-Au@Ag_2O images, we draw two conclusions. First, the large AlkP-Au@Ag_2O agglomerates have a core@shell structure. Second, the formation of large agglomerates depends on the presence of AlkP.

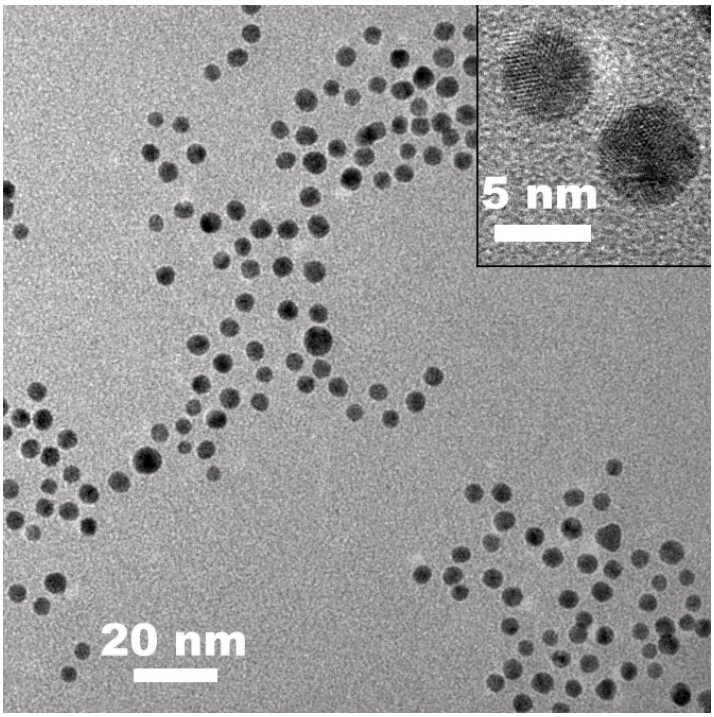

Figure 5.2. TEM micrograph of AlkP-Au. The Au colloid is dispersed and no core@shell morphology is observed. Inset: two AlkP-Au particles at a higher magnification.

UV-vis spectra for desalted, aqueous solutions of Au colloids, Au@Ag_2O, AlkP-Au, and AlkP-Au@Ag_2O are shown in Figure 5.3. Each spectrum was normalized to a maximum absorbance of 1.0 to facilitate comparison of the spectra. The Au colloid starting material has a peak centered at 523 nm, which corresponds to the plasmon reported for Au NPs in this size range.[95] The solution containing AlkP-Au is similar to that of the Au colloid solution except for a slight shift in the plasmon band to 527 nm.

The spectrum of Au@Ag_2O reveals the effect of Ag deposition onto the Au colloids. In this case, a new peak is observed at 410 nm, but the Au plasmon previously observed in the spectra of the Au colloid and AlkP-Au solutions is absent. The position of the new peak arising from Au@Ag_2O corresponds to a Ag plasmon, which has previously been reported in the literature for Ag colloids, Ag_2O thin films, and Ag NPs having a Ag_2O shell (Ag@Ag_2O).[96-98] The position of the peak observed for Au@Ag_2O is also similar to the plasmon band reported for bimetallic Au@Ag nanoparticles, in which the Au plasmon is quenched by the presence of the Ag (or Ag_2O) shell.[99-100] Accordingly, this finding is consistent with the core@shell structure revealed by the TEM images in Figure 5.1a.

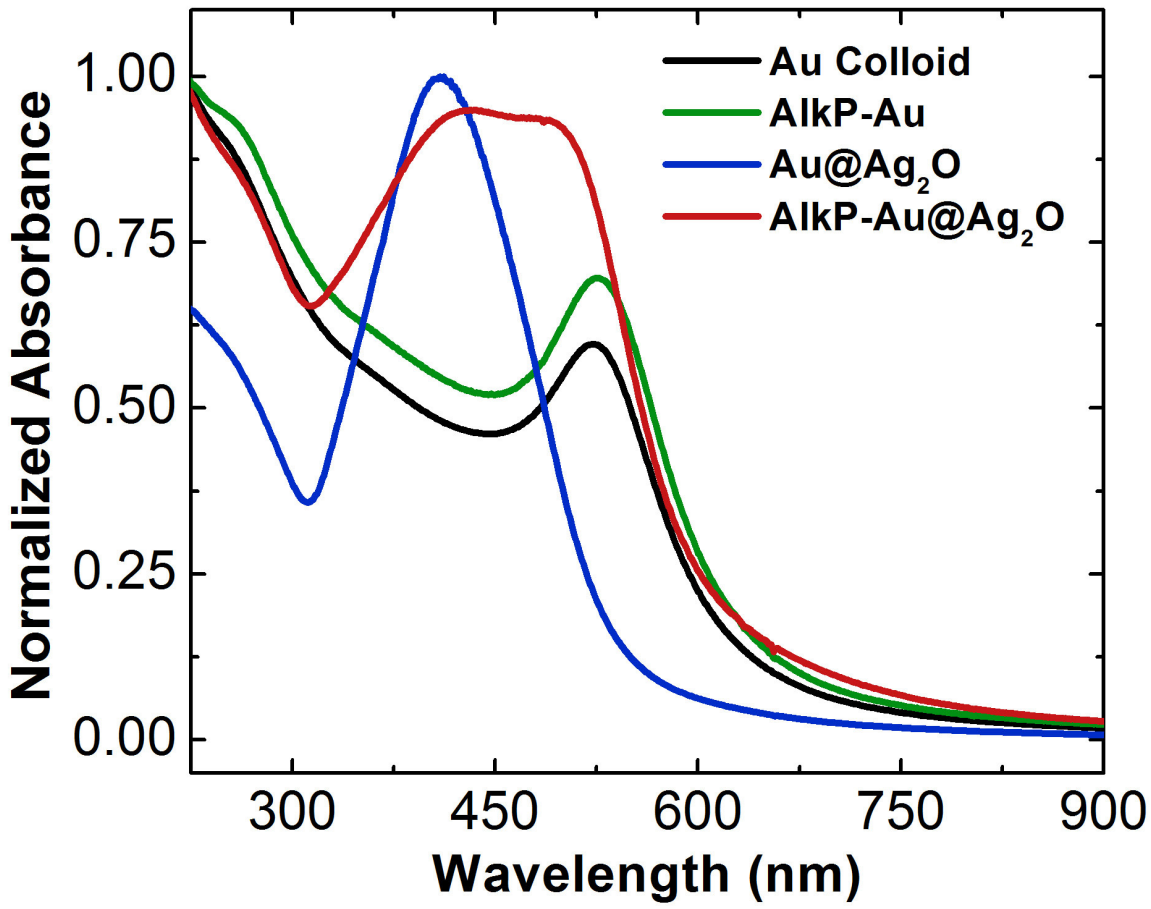

Figure 5.3. UV-vis spectra of desalted, aqueous solutions of Au colloids, AlkP-Au, Au@Ag_2O, and AlkP-Au@Ag_2O. The absorbance has been normalized to facilitate comparison of the spectra.

The spectrum of AlkP-Au@Ag_2O is different than the other three spectra in that it exhibits two overlapping peaks at 427 and 505 nm. The position of the 427 nm peak is consistent with Ag_2O. However, the presence of the peak at 505 nm suggests that some fraction of the Au surface, probably in the larger agglomerates (Figure 5.1b), is not covered with Ag_2O. This view is consistent with results reported by Gonzalez et al., who observed a similar spectrum for bimetallic Au@Ag nanoparticles having only a partial Ag shell.[99] Because protein adhesion to Au NPs is well documented,[101] we speculate that its presence is responsible for incomplete Ag_2O coverage and hence the band at 505 nm.

XPS analysis. C 1s XPS spectra collected for Au colloids, Au@Ag_2O, AlkP-Au@Ag_2O, and WT AlkP are provided in Figure 5.4. The high-resolution C spectra exhibit binding energies consistent with those reported for C-C, C-N, and C-O bonds.[58,57] For example, the C 1s spectrum for Au@Ag_2O consists of two peaks having binding energies corresponding to C-C and C-O bonds.[58] The presence of a C-O peak can be attributed to the citrate capping agent on the Au colloids. The spectrum of AlkP-Au@Ag_2O exhibits three dominant features.

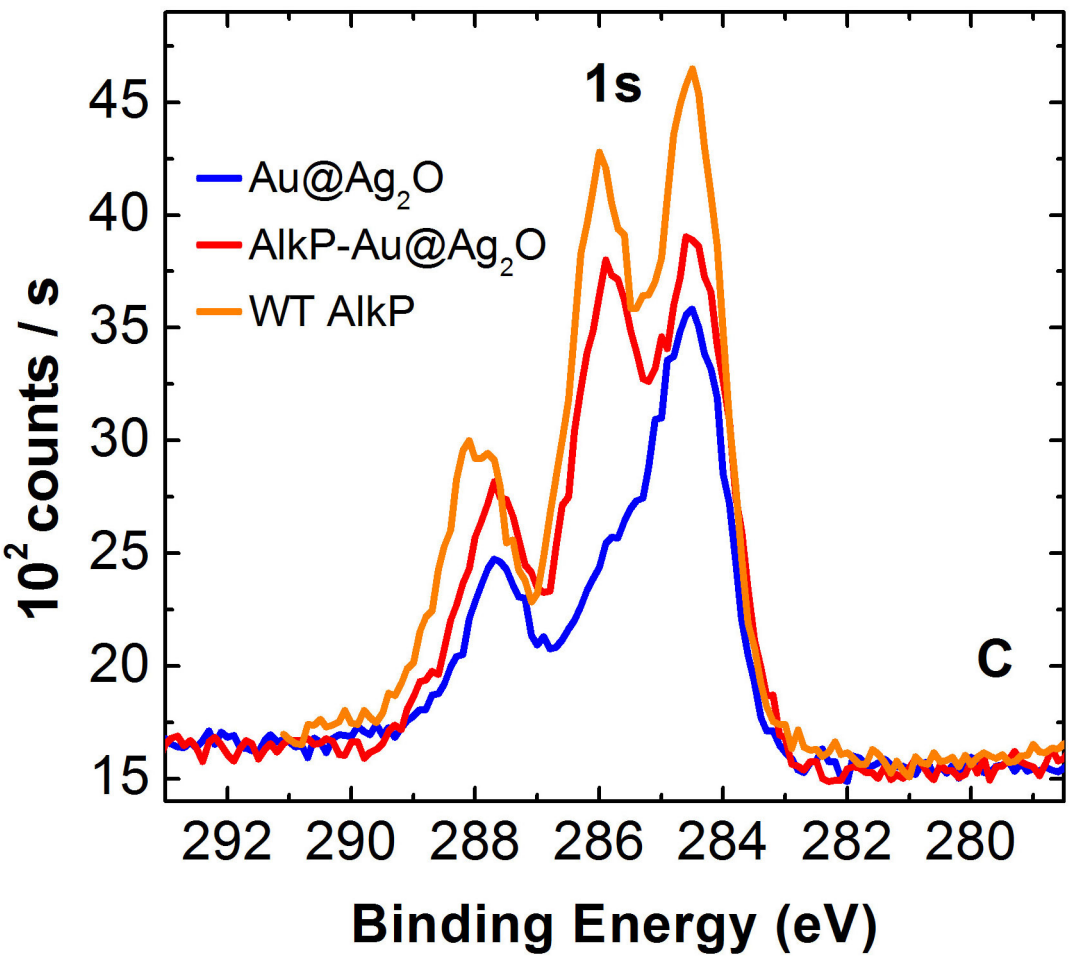

Figure 5.4. High-resolution C 1s XPS spectra for Au@Ag_2O, AlkP-Au@Ag_2O, and WT AlkP. The three features correspond to C-C (284.5 eV), C-N (286.0 eV), and C-O (287.5 eV) functional groups.

Two of these peaks have energies coincident with the C-C and C-O bonds in the Au@Ag_2O spectrum. The binding energy of the center peak in the AlkP-Au@Ag_2O spectrum is suggestive of C-N bonding. The three features also appear in WT AlkP. Recalling that the AlkP-Au@Ag_2O solution was washed and filtered to remove free enzyme prior to XPS analysis, we conclude that AlkP is entrapped within these Au@Ag_2O agglomerates.

The high-resolution Ag 3d XPS spectra of Au@Ag_2O and AlkP-Au@Ag_2O are provided in Figure 5.5. Dashed lines indicate the reported binding energies for zerovalent Ag (368.3 eV and 374.3 eV).[58-59] The $3d_{5/2}$ peaks for Au@Ag_2O and AlkP-Au@Ag_2O appear at 368.1 and 367.7 eV, respectively, which are somewhat lower than the corresponding literature value for zerovalent Ag.[58] However, these binding energies are consistent with values reported for Ag_2O (between 367.5-368.2 eV).[58,96,102] That Ag_2O has a more negative binding energy than zerovalent Ag is attributed to the electronic structure of Ag_2O and its metal-like conductivity.[103-104] We conclude that Ag_2O is the principal Ag species present in both Au@Ag_2O and AlkP-Au@Ag_2O. High-resolution XPS spectra in the Au region are provided in Figure 5.6 and indicate the presence of zerovalent Au only.

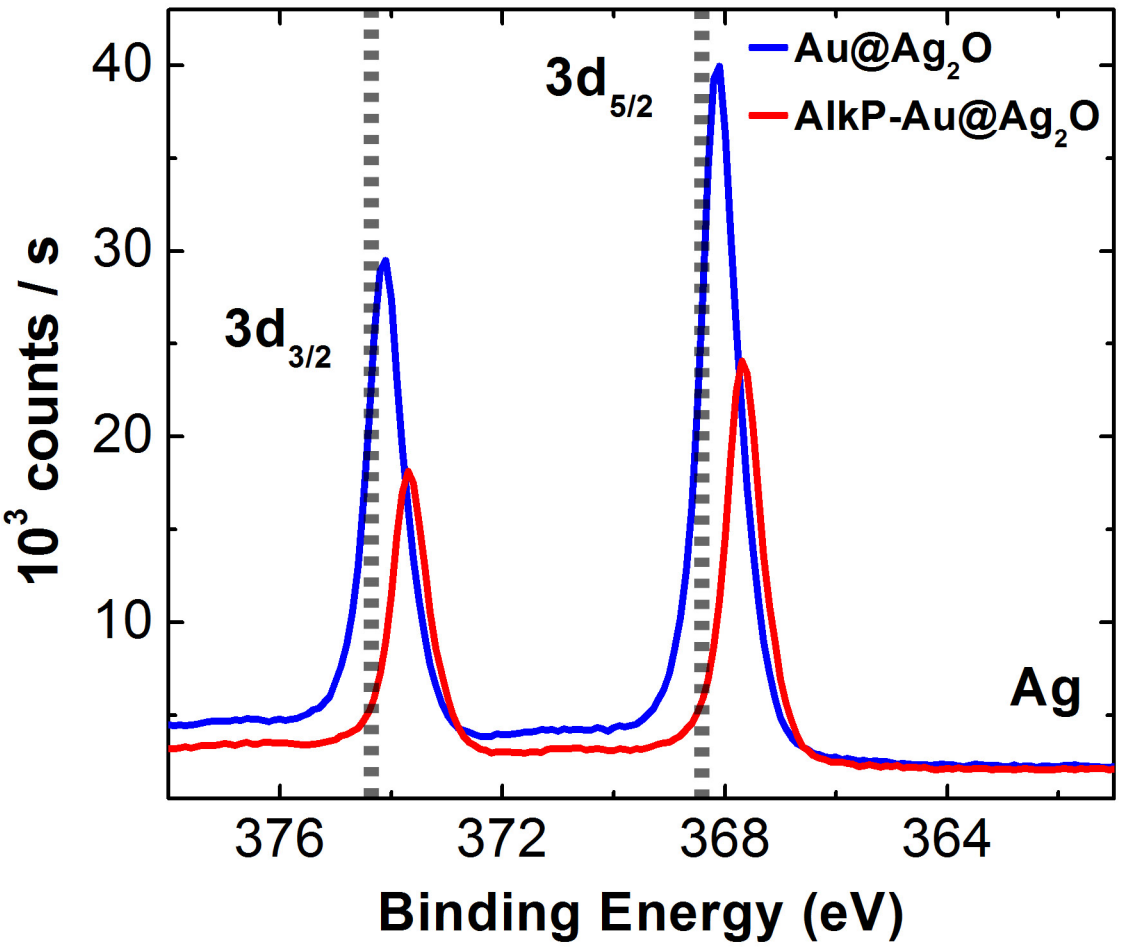

Figure 5.5. High-resolution XPS spectra of Ag 3d XPS spectra for $Au@Ag_2O$ and $AlkP\text{-}Au@Ag_2O$. The dashed lines show reference energies for Ag^0 for the $3d_{5/2}$ and $3d_{3/2}$ energies.

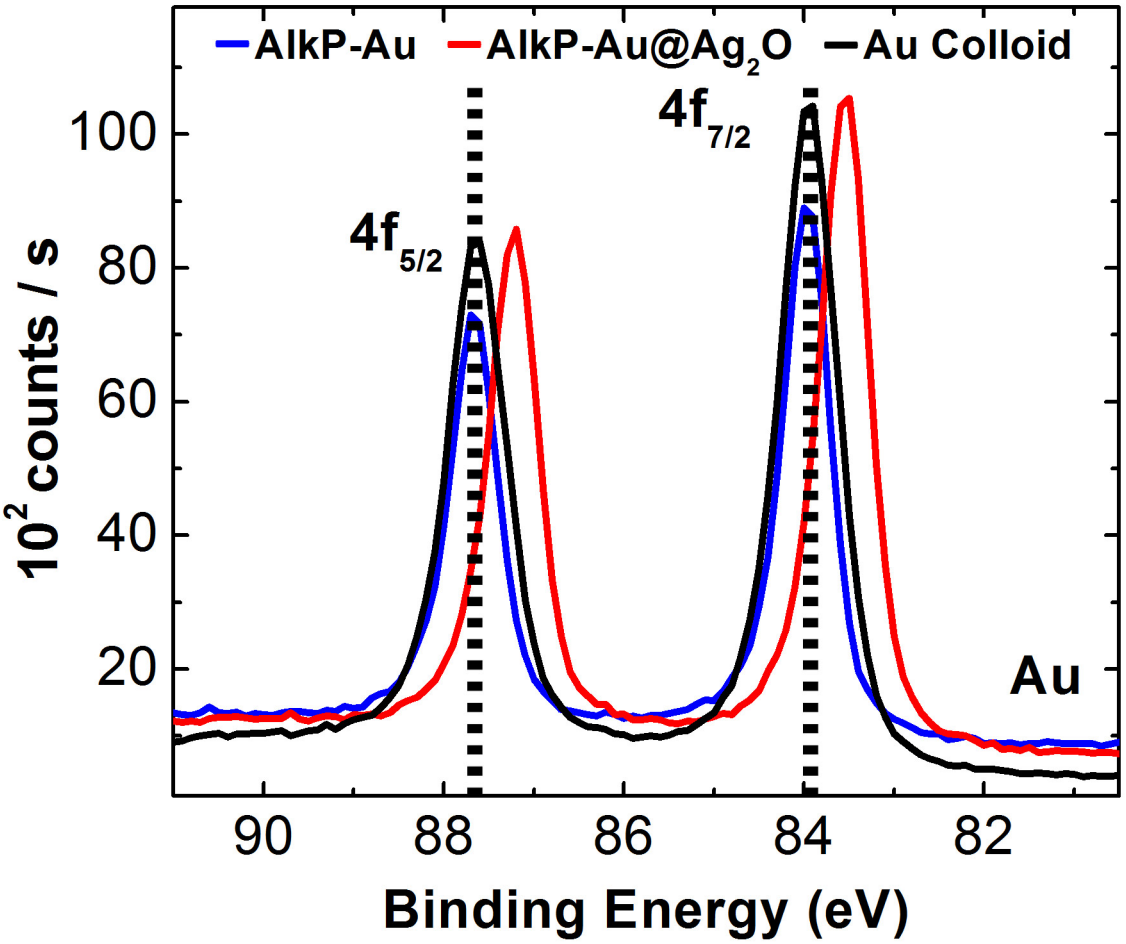

Figure 5.6. High-resolution XPS spectra of Au 4f XPS spectra for Au colloid, $Au@Ag_2O$, and $AlkP\text{-}Au@Ag_2O$. The dashed lines show reference energies for Au^0 for the $4f_{7/2}$ and $4f_{5/2}$ energies.

EDS mapping. We used element mapping to carry out spatially resolved analysis of the large AlkP-Au@Ag_2O agglomerates shown in Figure 5.1b. Figure 5.7 is a drift-corrected element map, rendered in false color, of a single agglomerate surrounded by several smaller particles. The inset is an STEM image of the EDS field of view. The map reveals two interesting features. First, the elemental distribution in the large agglomerate is consistent with that of a Au@Ag_2O core@shell morphology. Second, its Au core is much larger than the ~5 nm colloids, which were the initial source of Au. This indicates the presence of multiple Au colloids in the core.

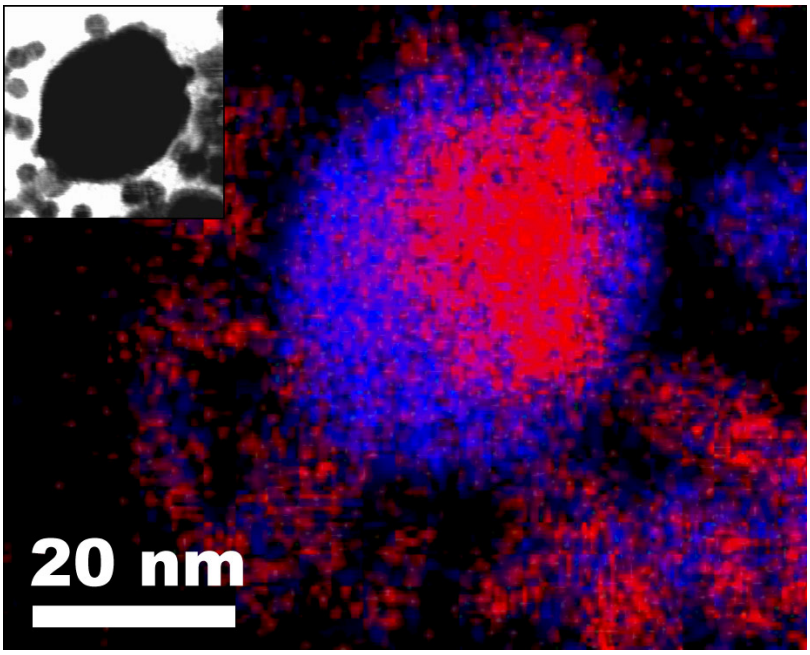

Figure 5.7. EDS element map of a AlkP-Au@Ag_2O agglomerate and smaller, nearby Au@Ag_2O particles. The image is rendered in false color: Ag is shown in blue and Au in red. The inset is an STEM image of the EDS field-of-view.

Activity assays and inhibition. Colorimetric activity assays were used to quantify the amount of AlkP present during each step of the synthesis of AlkP-Au@Ag_2O. The DEA assay described in the Experimental Section was selected to determine the AlkP concentration in activity units, because it reports an absolute quantity of the functional enzyme. As discussed earlier, the metal-containing solutions were purified to ensure that free AlkP was removed. This step is important for interpreting the activity assay, because it ensures that the measured activity arises only from AlkP associated with agglomerates. Filtration and washing steps were used for purification, and they result in three fractions. The initial filtrate consists of unbound AlkP, solvent, glycine, and salts that were introduced during the synthesis. The wash solution used to ensure removal of free AlkP from the retained solid material comprises the second fraction. Finally, the solid remaining after the wash step was taken up in water, and this represents the third fraction. The filtrate and wash fractions were pooled and analyzed for enzyme activity alongside the resuspended solid for each of the following samples: WT AlkP, Au@Ag_2O, AlkP-Au, and AlkP-Au@Ag_2O. Information about the analysis of these data is provided in the Experimental Section.

Species	Filtrate + Wash Activity	Pellet Activity	Overall Sum Activity
WT AlkP	1.647 ± 0.074	0.022 ± 0.003	1.668 ± 0.074 U
$Au@Ag_2O$	-0.001 ± 0.005	0.030 ± 0.046	0.029 ± 0.046 U
AlkP-Au	0.493 ± 0.066	0.874 ± 0.113	1.367 ± 0.131 U
AlkP-$Au@Ag_2O$	0.789 ± 0.049	0.206 ± 0.007	0.994 ± 0.049 U

Table 5.1. The active quantity of AlkP in DEA units (U) for the WT AlkP, $Au@Ag_2O$, AlkP-Au and AlkP-$Au@Ag_2O$ species by fraction. Activities were measured for the pooled filtrate plus wash fractions and the resuspended pellet. The total activity is shown in the column on the right. The values shown represent the average of 3-5 replicates carried out using independently prepared materials ($\pm 1\sigma$).

The results from the activity assays, in terms of catalytically active enzyme units (U), are presented in Table 1. For WT AlkP, we find that essentially all enzyme activity arises from the pooled filtrate and wash, which is consistent with expectations for filtration of a 60 kDa molecular weight enzyme through a 100 kDa MWCO filter. Also consistent with expectations, the enzyme-free Au@Ag_2O particles registered effectively zero activity.

The effect of NPs on the activity of the enzyme is revealed by the results of the AlkP-Au assay. Here, there is a decrease in the total enzyme activity compared to free WT AlkP, which is typical for enzymes adsorbed to metal surfaces.[105] Specifically, the total enzyme activity for the AlkP-Au material (pellet, filtrate, and wash, Table 1) is ~82% that of the total free WT enzyme. Analysis of AlkP-Au@Ag_2O fractions indicates that the majority of the enzyme is eluted in the filtrate and wash. In fact, somewhat surprisingly, there is more free enzyme observed with AlkP-Au@Ag_2O than with AlkP-Au. This could be due to displacement of AlkP from the Au surface during formation of the Ag_2O shell. Finally, we find that 13% of the AlkP activity is retained in AlkP-Au@Ag_2O compared to the total free WT AlkP. This is not a high degree of activity, but as we will see in the next section the 13% remaining is quite stable in the presence of inhibitors.

Inhibition assays. The activities of WT AlkP, AlkP-Au, and AlkP-Au@Ag_2O were quantified in the presence of

inhibitors to evaluate the stabilizing effect of the Ag_2O shell. The inhibition assays were performed in the same manner as the activity assay described in the previous section, except for the presence of the inhibitors urea or Phe. Urea is a denaturant that disrupts the secondary structure of AlkP.[47] Phe is an uncompetitive inhibitor that delays the release of product from AlkP.[49,106]

The normalized activities of AlkP, AlkP-Au, and AlkP-Au@Ag_2O in the presence of two different concentrations of urea and Phe are compared in Figure 5.8.

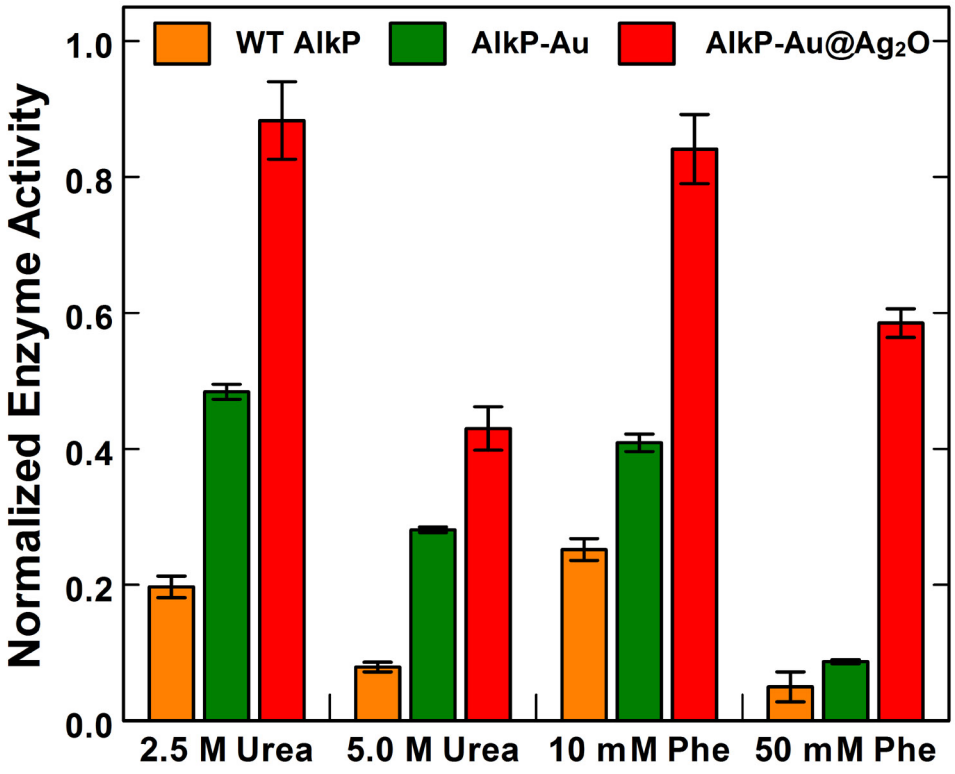

Figure 5.8. A histogram comparing inhibition data for WT AlkP, AlkP-Au, and AlkP-Au@Ag_2O in the presence of 2.5 and 5.0 M urea, and 10.0 and 50.0 mM Phe. Error bars represent ±1σ from the mean.

Different concentrations of enzyme were used for the WT AlkP, AlkP-Au, and AlkP-Au@Ag_2O assays, and therefore the results were normalized. The normalized enzyme activities shown in Figure 5.8 were calculated using the following equations:

$$E_{calc} = \frac{U_{fraction}}{U_{sum}}$$

Here, E_{calc} is the fraction of the total AlkP used for the inhibitor assay, $U_{fraction}$ is the activity of the fraction used for the assays (Table 5.1, first or second column, depending on the assay), and U_{sum} is the total activity for that species (Table 1, third column).

Normalized enzyme activity (NEA, vertical axis, Figure 5.8) is defined as follows.

$$NEA = \frac{U_{inhibited} / U_{initial}}{E_{calc}}$$

where $U_{inhibited}$ is the activity measured for the sample incorporating the inhibitor and $U_{initial}$ is the activity measured for the sample lacking the inhibitor.

WT AlkP was strongly inhibited in this assay, and exhibited a normalized activity of < 0.30 for urea and Phe at both concentrations. The normalized activity of AlkP-Au was found to be < 0.50 in all cases. These data indicate that the surface adsorption of AlkP onto Au colloids in AlkP-Au provides some protective benefit. However, a more notable enhancement in activity is observed for the enzyme in the form of AlkP-Au@Ag_2O. Indeed, AlkP-Au@Ag_2O remained

almost fully active in the presence of the dilute inhibitors, and even at the high inhibitor concentrations AlkP-Au@Ag_2O was more active than either WT AlkP or AlkP-Au. We conclude that the Ag_2O shell provides a significant degree of stability for AlkP in the presence of urea and Phe, while still providing access to the substrate used for the assay. Although we have only examined urea and Phe, it seems likely the approach described here will extend to other inhibitors.

5.5 Summary and Conclusions

We have described a means for stabilizing AlkP against two inhibitors: urea and Phe, which operate on the enzyme by different mechanisms. Structural characterization suggests that the enzyme is incorporated into a conductive Au@Ag_2O core@shell structure, but beyond this we are not prepared to discuss the molecular-level details that lead to stabilization. There are two aspects of the findings reported here that are significant. First, the stabilizing agent is electrically conductive, and therefore there is a chance that this approach, or one like it, could be used to stabilize redox enzymes and electrically wire them to an electrode surface. Second, the time required to prepare the AlkP-Au@Ag_2O construct is one day. This is significantly faster than has been reported previously for sol-gel and other types of enzyme stabilizers.[40-41,92]

Chapter 6. Summary and Conclusion

This dissertation presents the development of devices and methodologies for enzymatic biosensing using enzyme-mediated catalysis and galvanic processes to generate and amplify signals. Existing biosensors for glucose monitoring and pregnancy indication are commercial successes that are widely accepted and provide practical benefit to consumers. Diagnostic medicine has benefited greatly from biological and chemical advances in areas including immunoassays, enzyme inhibitors, and precise protein and DNA quantification. With greater advances comes a related increase in the level of infrastructure required to implement them. The central point of this dissertation is the development of materials and techniques for biosensing that can be carried out in settings without highly skilled technicians or complex instruments by employing enzymatic and galvanic reactions.

Chapter 3 described the development of a DNA sensor based on the enzymatic deposition of Ag to change the electrical resistance of a specially designed electrode. The electrode, an IDA, was patterned via photolithography to place two Au electrodes in close proximity separated by a long, thin, serpentine glass interstice. A capture-target assay was employed to first modify the Au surface with capture DNA. The hybridization of a biotin-modified target

allowed for the recruitment of alkaline phosphatase (AlkP). Biometallization was carried out using ascorbic acid and Tollen's reagent to deposit conductive Ag. Measuring the resistance with a multimeter gave a qualitative response to indicate detection. Dose-response assays showed this method was sensitive to 1 aM of target DNA. This concentration is approximately the same as the pathological amount of the actual Epstein Barr DNA found in serum.

Chapter 4 presented a self-powered trypsin sensor that yielded quantitative enzyme detection through the use a LED-equipped galvanic cell. The presence of this proteolytic enzyme in blood serum is associated with acute pancreatitis. The sensing platform was a $Mg//Fe^{3+}$ galvanic cell whose anode was obscured from solution by protein and Al barrier layers. Sensing was accomplished in two steps. First, the test solution was added to the anodic well where trypsin would degrade the protein. Second, a volume of hydroxide solution was added. A trypsin-digested gel allows hydroxide to reach and dissolve the Al faster than a gel not exposed to trypsin. Dose response experiments were carried out with trypsin in either buffer or serum and showed a relationship between the concentration of trypsin and the LED illumination time following hydroxide addition.

Chapter 5 explored the encapsulation of AlkP using core@shell nanoparticles of $Au@Ag_2O$. The Ag_2O was concluded to stabilize and protect AlkP against the inhibitory chemicals urea and Phe. Imaging and spectroscopic

characterizations suggest that AlkP strongly associates with citrate-capped Au colloid to endure washing, and that a Ag_2O shell forms while agglomerating several Au colloid particles together as the core. The activity of AlkP was quantified using a time-resolved colorimetric assay to determine that ~21% of the initial active enzyme is associated with the NPs, and when exposed to urea or Phe the AlkP-Au@Ag_2O species tolerate the chemicals to a greater extent than WT AlkP or Au-associated AlkP.

References

1. Weitgasser, R.; Gappmayer, B. New portable devices for blood glucose measurement: Comparison of MediSense card, Glucometer Elite, Hypocount Supreme and Omnican Control with the reference glucose oxidase method. *Schweiz. Med. Wochenschr.* **1997**, *127*, 12-17.
2. Bergmeyer, H. U.; Gawehn, K.; Grassl, M., *Enzymes as Biological Reagents*, in *Methods of Enzymatic Analysis*, H.U. Bergmeyer, Editor. 1974, Academic Press, Inc.: New York, NY. p. 515-516.
3. Kasana, R. C. Proteases from Psychrotrophs: An Overview. *Crit. Rev. Microbiol.* **2010**, *36*, 134-145.
4. *Trypsin*, in *Springer Handbook of Enzymes*, D. Schomberg and I. Schomberg, Editors. 2002, Springer-Verlag: New York. p. 11-24.
5. Rodríguez-López, J. N.; Lowe, D. J.; Hernández-Ruiz, J.; Hiner, A. N. P.; García-Cánovas, F.; Thorneley, R. N. F. Mechanism of Reaction of Hydrogen Peroxide with Horseradish Peroxidase: Identification of Intermediates in the Catalytic Cycle. *J. Am. Chem. Soc.* **2001**, *123*, 11838-11847.
6. Morton, R. K. Some properties of alkaline phosphatase of cow's milk and calf intestinal mucosa. *Biochem. J.* **1955**, *60*, 573-582.
7. Preechaworapun, A.; Dai, Z.; Xiang, Y.; Chailapakul, O.; Wang, J. Investigation of the enzyme hydrolysis

products of the substrates of alkaline phosphatase in electrochemical immunosensing. *Talanta* **2008**, *76*, 424-431.

8. Hwang, S.; Kim, E.; Kwak, J. Electrochemical detection of DNA hybridization using biometallization. *Anal. Chem.* **2005**, *77*, 579-584.
9. Taton, T. A.; Mirkin, C. A.; Letsinger, R. L. Scanometric DNA Array Detection with Nanoparticle Probes. *Science* **2000**, *289*, 1757-1760.
10. Chen, Z.-P.; Peng, Z.-F.; Jiang, J.-H.; Zhang, X.-B.; Shen, G.-L.; Yu, R.-Q. An electrochemical amplification immunoassay using biocatalytic metal deposition coupled with anodic stripping voltammetric detection. *Sens. Actuators, B* **2008**, *129*, 146-151.
11. Möller, R.; Powell, R. D.; Hainfeld, J. F.; Fritzsche, W. Enzymatic Control of Metal Deposition as Key Step for a Low-Background Electrical Detection for DNA Chips. *Nano Lett.* **2005**, *5*, 1475-1482.
12. Chidsey, C. E.; Feldman, B. J.; Lundgren, C.; Murray, R. W. Micrometer-Spaced Platinum Interdigitated Array Electrode - Fabrication, Theory, and Initial Use. *Anal. Chem.* **1986**, *58*, 601-607.
13. Dam, V. A. T.; Olthuis, W.; van den Berg, A. Redox cycling with facing interdigitated array electrodes as a method for selective detection of redox species. *Analyst* **2007**, *132*, 365-370.

14. Möller, R.; Csáki, A.; Köhler, J. M.; Fritzsche, W. Electrical Classification of the Concentration of Bioconjugated Metal Colloids after Surface Adsorption and Silver Enhancement. *Langmuir* **2001**, *17*, 5426-5430.

15. Ma, Y. F.; Zhang, J. M.; Zhang, G. J.; He, H. X. Polyaniline nanowires on Si surfaces fabricated with DNA templates. *J. Am. Chem. Soc.* **2004**, *126*, 7097-7101.

16. Sailor, M. J.; Curtis, C. L. Conducting Polymer Connections for Molecular Devices. *Adv. Mater.* **1994**, *6*, 688-692.

17. Murray, B. J.; Walter, E. C.; Penner, R. M. Amine Vapor Sensing with Silver Mesowires. *Nano Lett.* **2004**, *4*, 665-670.

18. VanGuilder, H. D.; Vrana, K. E.; Freeman, W. M. Twenty-five years of quantitative PCR for gene expression analysis. *BioTechniques* **2008**, *44*, 619-626.

19. Nam, J. M.; Stoeva, S. I.; Mirkin, C. A. Bio-Bar-Code-Based DNA Detection with PCR-like Sensitivity. *J. Am. Chem. Soc.* **2004**, *126*, 5932-5933.

20. Luo, Y.; Mao, X.; Peng, Z. F.; Jiang, J. H.; Shen, G. L.; Yu, R. Q. A new strategy for electrochemical immunoassay based on enzymatic silver deposition on agarose beads. *Talanta* **2008**, *74*, 1642-1648.

21. Liu, D. J.; Perdue, R. K.; Sun, L.; Crooks, R. M. Immobilization of DNA onto poly(dimethylsiloxane) surfaces and application to a microelectrochemical

enzyme-amplified DNA hybridization assay. *Langmuir* **2004**, *20*, 5905-5910.

22. Bard, A. J.; Faulkner, L. R. *Electrochemical methods: fundamentals and applications*; 2nd ed. John Wiley & Sons, Inc.: Hoboken, NJ, 2001.
23. Eggen, P. O.; Gronneberg, T.; Kvittingen, L. Small-scale and low-cost galvanic cells. *J. Chem. Educ.* **2006**, *83*, 1201-1203.
24. Faulkner, L. R.; Walsh, M. R.; Xu, C. J. *New Instrumental Approaches to Fast Electrochemistry at Ultramicroelectrodes*. Contemporary Electroanalytical Chemistry, ed. A. Ivaska, A. Lewenstam, and R. Sara. Plenum Press Div Plenum Publishing Corp: New York, 1990.
25. Walsh, K. A.; Gertrude, E. P.; Lorand, L., *Trypsinogens and trypsins of various species*, in *Methods Enzymol.* 1970, Academic Press. p. 41-63.
26. Artigas, J. M.; Garcia, M. E.; Faure, M. R.; Gimeno, A. M. Serum trypsin levels in acute pancreatic and non-pancreatic abdominal conditions. *Postgrad. Med. J.* **1981**, *57*, 219-222.
27. Ionescu, R. E.; Cosnier, S.; Marks, R. S. Protease Amperometric Sensor. *Anal. Chem.* **2006**, *78*, 6327-6331.
28. Johnston-Banks, F. A., *Gelatine*, in *Food Gels*, P. Harris, Editor. 1990, Elsevier Applied Science: New York. p. 233-289.

29. Veis, A.; Cohen, J. Reversible Transformation of Gelatin to the Collagen Structure. *Nature* **1960**, *186*, 720-721.
30. Mercadé-Prieto, R.; Chen, X. D. Dissolution of whey protein concentrate gels in alkali. *AIChE J.* **2006**, *52*, 792-803.
31. Mercadé-Prieto, R.; Falconer, R. J.; Paterson, W. R.; Wilson, D. I. Swelling and Dissolution of B-Lactoglobulin Gels in Alkali. *Biomacromolecules* **2007**, *8*, 469-476.
32. Mercadé-Prieto, R.; Gunasekaran, S. Alkali Cold Gelation of Whey Proteins. Part II: Protein Concentration. *Langmuir* **2009**, *25*, 5793-5801.
33. Mercadé-Prieto, R.; Paterson, W. R.; Dong Chen, X.; Ian Wilson, D. Diffusion of NaOH into a protein gel. *Chem. Eng. Sci.* **2008**, *63*, 2763-2772.
34. Ruben, M.-P.; William, R. P.; Wilson, D. I. Caustic-induced gelation of B-lactoglobulin. *Int. J. Food Sci. Technol.* **2008**, *43*, 1379-1386.
35. MP Biomedicals Trypsin Product Information. February 8, 2010. http://www.mpbio.com/product_info.php?family_key=02190046
36. Ionescu, R. E.; Fillit, C.; Jaffrezic-Renault, N.; Cosnier, S. Urease-gelatin interdigitated microelectrodes for the conductometric determination of

protease activity. *Biosens. Bioelectron.* **2008**, *24*, 489-492.

37. Lefkowitz, R. B.; Schmid-Schonbein, G. W.; Heller, M. J. Whole blood assay for trypsin activity using polyanionic focusing gel electrophoresis. *Electrophoresis* **2010**, *31*, 2442-2451.
38. Kim, J.; Grate, J. W.; Wang, P. Nanostructures for enzyme stabilization. *Chem. Eng. Sci.* **2006**, *61*, 1017-1026.
39. Park, B. W.; Yoon, D. Y.; Kim, D. S. Recent progress in bio-sensing techniques with encapsulated enzymes. *Biosens. Bioelectron.* **2010**, *26*, 1-10.
40. Braun, S.; Rappoport, S.; Zusman, R.; Avnir, D.; Ottolenghi, M. Biochemically Active Sol-Gel Glasses - the Trapping of Enzymes. *Mater. Lett.* **1990**, *10*, 1-5.
41. Smith, K.; Silvernail, N. J.; Rodgers, K. R.; Elgren, T. E.; Castro, M.; Parker, R. M. Sol Gel Encapsulated Horseradish Peroxidase: A Catalytic Material for Peroxidation. *J. Am. Chem. Soc.* **2002**, *124*, 4247-4252.
42. Li, Y. K.; Chou, M. J.; Wu, T. Y.; Jinn, T. R.; Chen-Yang, Y. W. A Novel method for preparing a protein-encapsulated bioaerogel: Using a red fluorescent protein as a model. *Acta Biomater.* **2008**, *4*, 725-732.
43. Wallace, J. M.; Rice, J. K.; Pietron, J. J.; Stroud, R. M.; Long, J. W.; Rolison, D. R. Silica Nanoarchitectures Incorporating Self-Organized Protein

Superstructures with Gas-Phase Bioactivity. *Nano Lett.* **2003**, *3*, 1463-1467.

44. Kim, J.; Grate, J. W. Single-Enzyme Nanoparticles Armored by a Nanometer-Scale Organic/Inorganic Network. *Nano Lett.* **2003**, *3*, 1219-1222.
45. Rangnekar, A.; Sarma, T. K.; Singh, A. K.; Deka, J.; Ramesh, A.; Chattopadhyay, A. Retention of Enzymatic Activity of α-Amylase in the Reductive Synthesis of Gold Nanoparticles. *Langmuir* **2007**, *23*, 5700-5706.
46. Ben-Knaz, R.; Avnir, D. Bioactive enzyme-metal composites: The entrapment of acid phosphatase within gold and silver. *Biomaterials* **2009**, *30*, 1263-1267.
47. Simopoulos, T. T.; Jencks, W. P. Alkaline Phosphatase Is an Almost Perfect Enzyme. *Biochemistry* **1994**, *33*, 10375-10380.
48. Walter, K.; Schuett, C., in *Methods of Enzymatic Analysis*, H.U. Bergmeyer, Editor. 1974, Academic Press, Inc.: New York. p. 860-864.
49. Ghosh, N. K.; Fishman, W. H. On the Mechanism of Inhibition of Intestinal Alkaline Phosphatase by l-Phenylalanine. *J. Biol. Chem.* **1966**, *241*, 2516-2522.
50. Fernley, H. N.; Walker, P. G. Inhibition of alkaline phosphatase by L-phenylalanine. *Biochem. J.* **1970**, *116*, 543-544.
51. Brunel, C.; Cathala, G. Imidazole - Inhibitor of L-Phenylalanine-Insensitive Alkaline-Phosphatases of

Tissues Other Than Intestine and Placenta. *Biochim. Biophys. Acta* **1972**, *268*, 415-421.

52. Suzuki, K.; Yoshimura, Y.; Hisada, Y.; Matsumoto, A. Sensitivity of Intestinal Alkaline-Phosphatase to L-Homoarginine and its Requation by Subunit-Subunit Interaction. *Jpn. J. Pharmacol.* **1994**, *64*, 97-102.
53. Williams, K. R.; Gupta, K.; Wasilik, M. Etch rates for micromachining processing-Part II. *J. Microelectromech. Syst.* **2003**, *12*, 761-778.
54. Dziunikowski, B. *Energy Dispersive X-ray Fluorescence Analysis*. Comprehensive Analytical Chemistry, ed. G. Svehla. Elsevier: New York, 1989.
55. Moseley, H. G. J. The High-Frequency Spectra of the Elements. *Phil. Mag. 6.* **1913**, *26*, 1024-1034.
56. Barr, T. L. *Modern ESCA : the principles and practice of x-ray photoelectron spectroscopy*. CRC Press: Boca Raton, 1994.
57. Heinrich, K. F. J. *Electron Beam X-Ray Microanalysis*. Van Nostrand Reinhold Company: New York, 1981.
58. Moulder, J. F.; Bomben, K. D.; Sobol, P. E.; Stickle, W. F. *Handbook of X-ray Photoelectron Spectroscopy*. Physical Electronics USA, Inc: Chigasaki, Japan, 1995.
59. Seah, M. P. Post-1989 calibration energies for X-ray photoelectron spectrometers and the 1990 Josephson constant. *Surf. Interface Anal.* **1989**, *14*, 488.

60. Hwang, S.; Kim, E.; Kwak, J. Electrochemical detection of DNA hybridization using biometallization. *Anal. Chem.* **2005**, *77*, 579-584.

61. Chen, Z.-P.; Peng, Z.-F.; Jiang, J.-H.; Zhang, X.-B.; Shen, G.-L.; Yu, R.-Q. An electrochemical amplification immunoassay using biocatalytic metal deposition coupled with anodic stripping voltammetric detection. *Sens. Actuators B: Chem.* **2008**, *129*, 146-151.

62. Limoges, B.; Marchal, D.; Mavré, F.; Savéant, J.-M.; Schöllhorn, B. Theory and Practice of Enzyme Bioaffinity Electrodes. Direct Electrochemical Product Detection. *J. Am. Chem. Soc.* **2008**, *130*, 7259-7275.

63. Luo, Y.; Mao, X.; Peng, Z. F.; Jiang, J. H.; Shen, G. L.; Yu, R. Q. A new strategy for electrochemical immunoassay based on enzymatic silver deposition on agarose beads. *Talanta* **2008**, *74*, 1642-8.

64. Festag, G.; Schuler, T.; Möller, R.; Csáki, A.; Fritzsche, W. Growth and Percolation of Metal Nanostructures in Electrode Gaps Leading to Conductive Paths for Electrical DNA Analysis. *Nanotechnology* **2008**, 125303-125312.

65. Park, S.-J.; Taton, T. A.; Mirkin, C. A. Array-Based Electrical Detection of DNA with Nanoparticle Probes. *Science* **2002**, *295*, 1503-1506.

66. Urban, M.; Möller, R.; Fritzsche, W. A paralleled readout system for an electrical DNA-hybridization

assay based on a microstructured electrode array. *Rev. Sci. Instrum.* **2003**, *74*, 1077-1081.

67. Möller, R.; Csáki, A.; Kohler, J. M.; Fritzsche, W. Electrical Classification of the Concentration of Bioconjugated Metal Colloids after Surface Adsorption and Silver Enhancement. *Langmuir* **2001**, *17*, 5426-5430.
68. Bange, A.; Halsall, H. B.; Heineman, W. R. Microfluidic immunosensor systems. *Biosens. Bioelectron.* **2005**, *20*, 2488-2503.
69. Carpini, G.; Lucarelli, F.; Marrazza, G.; Mascini, M. Oligonucleotide-modified screen-printed gold electrodes for enzyme-amplified sensing of nucleic acids. *Biosens. Bioelectron.* **2004**, *20*, 167-175.
70. Feng, K.; Li, J. S.; Jiang, J. H.; Shen, G. L.; Yu, R. Q. QCM detection of DNA targets with single-base mutation based on DNA ligase reaction and biocatalyzed deposition amplification. *Biosens. Bioelectron.* **2007**, *22*, 1651-1657.
71. Liao, M. L.; Seib, P. A. A Stable Form of Vitamin-C - L-Ascorbate 2-Triphosphate - Synthesis, Isolation, and Properties. *J. Agric. Food Chem.* **1990**, *38*, 355-366.
72. Anker, P.; Stroun, M.; Maurice, P. A. Spontaneous Release of DNA by Human-Blood Lymphocytes as Shown in an In-Vitro System. *Cancer Res.* **1975**, *35*, 2375-2382.
73. Chang, C. P. Y.; Chia, R. H.; Wu, T. L.; Tsao, K. C.; Sun, C. F.; Wu, J. T. Elevated cell-free serum DNA

detected in patients with myocardial infarction. *Clin. Chim. Acta* **2003**, *327*, 95-101.

74. Vlassov, V. V.; Laktionov, P. P.; Rykova, E. Y. Extracellular nucleic acids. *BioEssays* **2007**, *29*, 654-667.

75. Baer, R.; Bankier, A. T.; Biggin, M. D.; Deininger, P. L.; Farrell, P. J.; Gibson, T. J.; Hatfull, G.; Hudson, G. S.; Satchwell, S. C.; Seguin, C.; Tuffnell, P. S.; Barrell, B. G. DNA sequence and expression of the B95-8 Epstein-Barr virus genome. *Nature* **1984**, *310*, 207-211.

76. Lo, Y. M. D.; Chan, L. Y. S.; Lo, K.-W.; Leung, S.-F.; Zhang, J.; Chan, A. T. C.; Lee, J. C. K.; Hjelm, N. M.; Johnson, P. J.; Huang, D. P. Quantitative Analysis of Cell-free Epstein-Barr Virus DNA in Plasma of Patients with Nasopharyngeal Carcinoma. *Cancer Res.* **1999**, *59*, 1188-1191.

77. Chidsey, C. E.; Feldman, B. J.; Lundgren, C.; Murray, R. W. Micrometer-Spaced Platinum Interdigitated Array Electrode - Fabrication, Theory, and Initial Use. *Anal. Chem.* **1986**, *58*, 601-607.

78. Pinneau, S. R. A Technique for Making One-Way Mirrors. *Child Development* **1951**, *22*, 235-241.

79. Morgan, R.; Myers, R. D. A study of chemically deposited silver mirrors. *J. Franklin Inst.* **1948**, *246*, 363-376.

80. Fukuyo, T.; Imai, H. Morphological evolution of silver crystals produced by reduction with ascorbic acid. *J. Cryst. Growth* **2002**, *241*, 193-199.

81. Jeohn, G.-H.; Serizawa, S.; Iwamatsu, A.; Takahashi, K. Isolation and Characterization of Gastric Trypsin from the Microsomal Fraction of Porcine Gastric Antral Mucosa. *J. Biol. Chem.* **1995**, *270*, 14748-14755.

82. *Trypsin*, in *Springer Handbook of Enzymes*, D. Schomberg and I. Schomberg, Editors. 2002. p. 11-24.

83. Regner, S.; Manjer, J.; Appelros, S.; Hjalmarsson, C.; Sadic, J.; Borgstrom, A. Protease activation, pancreatic leakage, and inflammation in acute pancreatitis: differences between mild and severe cases and changes over the first three days. *Pancreatology* **2008**, *8*, 600-607.

84. Katz, E.; Bückmann, A. F.; Willner, I. Self-Powered Enzyme-Based Biosensors. *J. Am. Chem. Soc.* **2001**, *123*, 10752-10753.

85. Germain, M. N.; Arechederra, R. L.; Minteer, S. D. Nitroaromatic Actuation of Mitochondrial Bioelectrocatalysis for Self-Powered Explosive Sensors. *J. Am. Chem. Soc.* **2008**, *130*, 15272-15273.

86. Streicher, M. A. Dissolution of Aluminum in Sodium Hydroxide Solutions - Effect of Gelatin and Potassium Permanganate. *Ind. Eng. Chem.* **1949**, *41*, 818-819.

87. Howell, B. A.; Cobb, V. S.; Haaksma, R. A. A convenient salt bridge for electrochemical experiments in the

general chemistry laboratory. *J. Chem. Educ.* **1983**, *60*, 273.

88. Finer, E. G.; Franks, F.; Phillips, M. C.; Suggett, A. Gel Formation from Solutions of Single-Chain Gelatin. *Biopolymers* **1975**, *14*, 1995-2005.

89. Foegeding, E. A.; Davis, J. P.; Doucet, D.; McGuffey, M. K. Advances in modifying and understanding whey protein functionality. *Trends Food Sci. Technol.* **2002**, *13*, 151-159.

90. Zaccheo, B. A.; Crooks, R. M. Detection of an Epstein Barr Genome Analog at Physiological Concentrations via the Biometallization of Interdigitated Array Electrodes. *Anal. Chem.* **2009**, *81*, 5757-5761.

91. Li, Y. K.; Chou, M. J.; Wu, T. Y.; Jinn, T. R.; Chen-Yang, Y. W. A Novel method for preparing a protein-encapsulated bioaerogel: Using a red fluorescent protein as a model. *Acta Biomater.* **2008**, *4*, 725-732.

92. Kumar, R.; Maitra, A. N.; Patanjali, P. K.; Sharma, P. Hollow gold nanoparticles encapsulating horseradish peroxidase. *Biomaterials* **2005**, *26*, 6743-6753.

93. Enzymatic Assay of PHOSPHATASE, ALKALINE. January 20, 2011. http://www.sigmaaldrich.com/etc/medialib/docs/Sigma/Enzyme_Assay/phosphalkeieth.Par.0001.File.dat/phosphalkeieth.pdf

94. Hamaguchi, K.; Kawasaki, H.; Arakawa, R. Photochemical synthesis of glycine-stabilized gold nanoparticles and its heavy-metal-induced aggregation behavior. *Colloids Surf., A* **2010**, *367*, 167-173.

95. Perrault, S. D.; Chan, W. C. W. Synthesis and Surface Modification of Highly Monodispersed, Spherical Gold Nanoparticles of 50 200 nm. *J. Am. Chem. Soc.* **2009**, *131*, 17042-17043.

96. Chiu, Y.; Rambabu, U.; Hsu, M. H.; Shieh, H. P. D.; Chen, C. Y.; Lin, H. H. Fabrication and nonlinear optical properties of nanoparticle silver oxide films. *J. Appl. Phys.* **2003**, *94*, 1996-2001.

97. Schinca, D. C.; Scaffardi, L. B.; Videla, F. A.; Torchia, G. A.; Moreno, P.; Roso, L. Silver-silver oxide core-shell nanoparticles by femtosecond laser ablation: core and shell sizing by extinction spectroscopy. *J. Phys. D.* **2009**, *42*, 215102-215111.

98. Soukupova, J.; Kvitek, L.; Kratochvilova, M.; Panacek, A.; Prucek, R.; Zboril, R. Silver Voyage from Macro- to Nanoworld. *J. Chem. Educ.* **2010**, *87*, 1094-1097.

99. Gonzalez, C. M.; Liu, Y.; Scaiano, J. C. Photochemical Strategies for the Facile Synthesis of Gold Silver Alloy and Core Shell Bimetallic Nanoparticles. *J. Phys. Chem. C* **2009**, *113*, 11861-11867.

100. Wilson, O. M.; Scott, R. W. J.; Garcia-Martinez, J. C.; Crooks, R. M. Synthesis, Characterization, and Structure-Selective Extraction of 1 3-nm Diameter AuAg

Dendrimer-Encapsulated Bimetallic Nanoparticles. *J. Am. Chem. Soc.* **2004**, *127*, 1015-1024.

101. Zhang, D.; Neumann, O.; Wang, H.; Yuwono, V. M.; Barhoumi, A.; Perham, M.; Hartgerink, J. D.; Wittung-Stafshede, P.; Halas, N. J. Gold Nanoparticles Can Induce the Formation of Protein-based Aggregates at Physiological pH. *Nano Lett.* **2009**, *9*, 666-671.
102. Hammond, J. S.; Gaarenstroom, S. W.; Winograd, N. X-ray photoelectron spectroscopic studies of cadmium- and silver-oxygen surfaces. *Anal. Chem.* **1975**, *47*, 2193-2199.
103. Deb, A.; Chatterjee, A. K. The electronic structure and chemical bonding mechanism of silver oxide. *J. Phys.: Condens. Matter* **1998**, *10*, 11719-11729.
104. Raju, N. R. C.; et al. Physical properties of silver oxide thin films by pulsed laser deposition: effect of oxygen pressure during growth. *J. Phys. D.* **2009**, *42*, 135411-135417.
105. Suckling, C. J. Immobilized enzymes. *Chem. Soc. Rev.* **1977**, *6*, 215-233.
106. Fernley, H. N.; Walker, P. G. Inhibition of alkaline phosphatase by L-phenylalanine. *Biochem. J.* **1970**, *116*, 543-544.

Vita

Brian Andrew Zaccheo received his Bachelor of Science degree from Boston College in 2005. He is expected to receive his doctorate degree in Biochemistry in the laboratory of Dr. Richard M. Crooks from The University of Texas at Austin in August 2011.

This dissertation was typed by Brian Andrew Zaccheo